

Asymptotic correlation functions in the Q -state Potts model: a universal form for point group C_{4v}

Masafumi Fujimoto¹ and Hiromi Otsuka²

¹Department of Physics, Nara Medical University, Kashihara, Nara 634-8521, Japan

²Department of Physics, Tokyo Metropolitan University, Tokyo 192-0397, Japan

E-mail: mfujimot@naramed-u.ac.jp

10 September 2019

Abstract. We consider the Q -state Potts model on the square lattice. Reexamining exact solutions of the Ising model ($Q = 2$), we propose a universal form for C_{4v} to analyze asymptotic correlation functions of off-critical systems. In contrast to the Ornstein-Zernicke form, it permits us to investigate the anisotropic correlation lengths (ACLs). Monte Carlo (MC) simulations are performed using the cluster algorithm proposed by Evertz and von der Linden. Fitting the MC data above the critical temperature with the universal form, we reproduce the ACL of the Ising model within a five-digit accuracy. Subsequently, for $Q = 3, 4$ above critical temperatures, we also obtain strong numerical evidence that the form is applicable to their asymptotic correlation functions and the ACLs. Furthermore, we apply it to the bond percolation problem which corresponds to the $Q \rightarrow 1$ limit. From the calculated ACLs, the equilibrium crystal shapes (ECSs) are derived via duality and Wulff's construction. Regarding Q as a continuous variable, we find that the ECS of the Q -state Potts model is essentially the same as those of the Ising model on the Union Jack and 4-8 lattices, which are represented as a simple algebraic curve of genus 1.

Keywords: Potts model, bond percolation, Monte Carlo simulation, anisotropic correlation length, equilibrium crystal shape, algebraic curve

PACS numbers: 05.50.+q, 05.10.Ln, 02.10.De, 61.50.Ah

Submitted to: *J. Phys. A: Math. Theor.*

1. Introduction

Thermal evolution of the equilibrium crystal shape (ECS) [1, 2] has received considerable attention for the last few decades [3, 4, 5, 6, 7, 8, 9, 10]. This revived interest is based on connections between the ECS and the roughening transition phenomena [2, 3, 4, 5, 6, 7]. The first exact analysis of the ECS was done for the square-lattice Ising model [3]; see also [4, 5].

Here, we investigate the two-dimensional (2D) Q -state Potts model [11, 12], whose Hamiltonian is described by the Q -valued variables $q_{\mathbf{r}}$:

$$E(Q) = - \sum_{\langle \mathbf{r}, \mathbf{r}' \rangle} J_{\mathbf{r}, \mathbf{r}'} \delta(q_{\mathbf{r}}, q_{\mathbf{r}'}), \quad q_{\mathbf{r}} = 0, 1, \dots, Q - 1. \quad (1.1)$$

The sum runs over all nearest-neighbor-site pairs $\langle \mathbf{r}, \mathbf{r}' \rangle$ on a lattice. Note that the $Q = 2$ Potts model is equivalent to the Ising model. For general Q , the Q -state Potts model is exactly solvable at the phase transition point [11, 13, 14, 15]. The phase transition is continuous for $Q \leq 4$, and first-order for $Q > 4$. In a previous study [8] we generalized the argument in [3, 4, 5] to find the ECS in the Q -state Potts model on the square lattice. We showed that the anisotropic correlation length (ACL) is related by duality [16, 17, 18, 19] to the anisotropic interfacial tension. For $Q > 4$, the ACL was exactly calculated at the first-order transition (or self-dual) point. The ECS was obtained from the ACL via the duality relation and Wulff's construction [1, 2]. It was expressed as an algebraic curve in the $\alpha\beta$ -plane

$$\alpha^2 \beta^2 + 1 + A_3(\alpha^2 + \beta^2) + A_4 \alpha \beta = 0, \quad (1.2)$$

where $\alpha = \exp[-\lambda(X+Y)/k_B T]$ and $\beta = \exp[-\lambda(X-Y)/k_B T]$ with the position vector (X, Y) of a point on the ECS and a suitable scale factor λ ; for definitions of A_3 and A_4 , see section 3.2 of [8]. The algebraic curve (1.2) is quite universal because it appears as the ECSs of a wide class of lattice models, including the square-lattice Ising model [3, 4, 5, 6, 7, 8, 9, 10].

We note that (1.2) is not the only universal curve [20, 21]. For example, we considered the ACL of the square-lattice eight-vertex model in [22]. It was shown that for a given x ($0 < x < 1$) there are two cases with respect to a parameter q . For $0 < q < x^3$, the ACL is written using the algebraic curve (1.2). However, for $x^3 < q < x^4$, the ACL is not related to (1.2), but to the algebraic curve

$$\alpha^2 \beta^2 + 1 + \bar{A}_2(\alpha\beta + 1)(\alpha + \beta) + \bar{A}_3(\alpha^2 + \beta^2) + \bar{A}_4 \alpha \beta = 0, \quad (1.3)$$

where \bar{A}_2 , \bar{A}_3 , and \bar{A}_4 are given by (4.7) of [22]. The ACL represented by (1.3) is the same as those of the Ising model on the Union Jack and 4-8 lattices [23]. Some authors derived algebraic curves for lattice models possessing six-fold rotational symmetry [23, 24, 25, 26, 27, 28], which are also general ones.

These algebraic curves are expected to be closely connected with symmetries of lattice models. How do symmetries select the algebraic curves? This is the problem we must consider. It is also expected that the same situation occurs regardless of whether the lattice models are exactly solvable.

In this paper, we propose a form to analyze asymptotic behavior of correlation functions of off-critical systems by reexamining exact solutions of the square-lattice Ising model. We investigate the asymptotic correlation functions observed in the Q -state Potts model. Our new approach is a combined use of the analytic form and the Monte Carlo (MC) method based on the Fortuin-Kasteleyn random-cluster representation [29]. It is known that the cluster representation works efficiently in small Q cases. The combined use is expected to be quite effective to calculate the asymptotic correlation function and the ACL.

The format of the present paper is as follows: In section 2, we define the Ising model on a rotated square lattice to investigate an effect of the C_{4v} symmetry on the asymptotic behavior of the correlation function. In section 3, we introduce the new idea, i.e., a form for the asymptotic correlation functions which together with the MC simulation data enables us to evaluate the ACLs. We apply it to the $Q = 2, 3$, and 4 cases, and also to the bond percolation model, which is, via the cluster representation, realized as the Potts model in the $Q \rightarrow 1$ limit. Section 4 is devoted to discussion and summary. The detailed explanations on limiting functions to appear in section 2.2, on the methodology of MC simulation calculations, and on the fitting procedure are given in appendices.

2. Exact analysis and elliptic curve in asymptotic correlation functions

In this section, we analyze the square-lattice Ising model [11, 30]. While the correlation function was studied by the Pfaffian method [31], we re-derive their results using a method that introduces the shift operator into the usual transfer matrix argument [22, 32] (see also [33, 34]). To find a role of the C_{4v} symmetry, we analyze the Ising model defined on a square lattice rotated through an arbitrary angle with respect to the coordinate axes.

2.1. Exact analysis: commuting transfer matrices

We consider the Hamiltonian (1.1) with $Q = 2$ defined on the square lattice Λ_{sq} . On each site $\mathbf{r} = i\mathbf{e}_x + j\mathbf{e}_y \in \Lambda_{\text{sq}}$, we introduce a spin variable as $\sigma_{\mathbf{r}} = \exp(2\pi i q_{\mathbf{r}}/Q)$. For $Q = 2$, $\sigma_{\mathbf{r}} = \pm 1$, so $\delta(q_{\mathbf{r}}, q_{\mathbf{r}'}) = \frac{1}{2}(1 + \sigma_{\mathbf{r}}\sigma_{\mathbf{r}'})$. Thus, the $Q = 2$ Potts model (with $J_{\mathbf{r},\mathbf{r}'}$ replaced by $2J_{\mathbf{r},\mathbf{r}'}$) is equivalent to the Ising model, whose Hamiltonian is given by

$$E = - \sum_{\mathbf{r}} (J\sigma_{\mathbf{r}+\mathbf{e}_x}\sigma_{\mathbf{r}} + J'\sigma_{\mathbf{r}+\mathbf{e}_y}\sigma_{\mathbf{r}}), \quad (2.1)$$

where nearest-neighbor spins are coupled by J or J' depending on the direction. We assume $J, J' > 0$. The partition function of the Ising model is

$$Z = \sum_{\sigma} \exp \left[\sum_{\mathbf{r}} (K\sigma_{\mathbf{r}+\mathbf{e}_x}\sigma_{\mathbf{r}} + K'\sigma_{\mathbf{r}+\mathbf{e}_y}\sigma_{\mathbf{r}}) \right], \quad (2.2)$$

where the outer sum is over all the spin configurations and the reduced couplings $K = J/k_{\text{B}}T$ and $K' = J'/k_{\text{B}}T$.

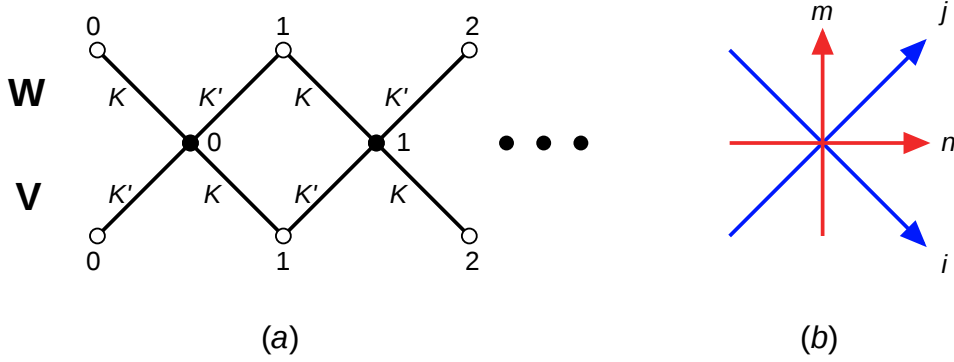


Figure 1. (a) Three successive rows of the square lattice drawn diagonally. (b) The transfer matrix \mathbf{U} operates spins on a row to transfer it from the lower to the upper direction along the m -axis. The i and j -axes correspond to the directions of the primitive translation vectors \mathbf{e}_x and \mathbf{e}_y of Λ_{sq} , respectively.

We introduce diagonal-to-diagonal transfer matrices: Consider two successive rows, and let $\sigma = \{\sigma_0, \sigma_1, \dots, \sigma_{N-1}\}$ (respectively $\sigma' = \{\sigma'_0, \sigma'_1, \dots, \sigma'_{N-1}\}$) be the spins in the lower (respectively upper) row. We assume the periodic boundary conditions in both directions. Then, as shown in figure 1(a), the transfer matrices \mathbf{V} and \mathbf{W} are defined by elements as

$$\begin{aligned} [\mathbf{V}]_{\sigma, \sigma'} &= \exp \left[\sum_{l=0}^{N-1} (K \sigma_{l+1} \sigma'_l + K' \sigma_l \sigma'_l) \right], \\ [\mathbf{W}]_{\sigma, \sigma'} &= \exp \left[\sum_{l=0}^{N-1} (K \sigma_l \sigma'_l + K' \sigma_l \sigma'_{l+1}) \right], \end{aligned} \quad (2.3)$$

where $\sigma_N = \sigma_0$ and $\sigma'_N = \sigma'_0$ (see chapter 7 of [11]). When the system has $2M$ rows, the partition function is given as follows:

$$Z = \text{Tr} \mathbf{U}^M = \sum_{p=1}^{2^N} (\Lambda_p^2)^M, \quad \mathbf{U} = \mathbf{V}\mathbf{W}, \quad (2.4)$$

where Λ_p^2 is the p -th eigenvalue of \mathbf{U} .

Above the critical temperature $T > T_C$, we parameterize K, K' using the elliptic functions with the modulus $k \in (0, 1)$ as

$$\begin{aligned} \sinh 2K &= \frac{k \text{sn}(iu)}{i}, & \cosh 2K &= \text{dn}(iu), \\ \sinh 2K' &= \frac{i}{\text{sn}(iu)}, & \cosh 2K' &= i \frac{\text{cn}(iu)}{\text{sn}(iu)}. \end{aligned} \quad (2.5)$$

I, I' are the quarter-periods, and the argument u satisfies the condition $0 < u < I'$ (see chapter 15 of [11]). For $T < T_C$, we can find the similar parameterization:

$$\begin{aligned} \sinh 2K &= \frac{\text{sn}(iu)}{i}, & \cosh 2K &= \text{cn}(iu), \\ \sinh 2K' &= \frac{i}{k \text{sn}(iu)}, & \cosh 2K' &= i \frac{\text{dn}(iu)}{k \text{sn}(iu)} \end{aligned} \quad (2.6)$$

(see also [35]).

Regard k as a fixed constant, and u as a complex variable. Then, it is obvious from (2.5) or (2.6) that \mathbf{U} is a function of u . When we write it as $\mathbf{U}(u)$, it satisfies the commutation relation

$$[\mathbf{U}(u), \mathbf{U}(u')] = 0 \quad \forall u, u' \in \mathbb{C}. \quad (2.7)$$

Further, let the spin reversal operator \mathbf{R} be the matrix with elements

$$[\mathbf{R}]_{\sigma, \sigma'} = \delta(\sigma_0, -\sigma'_0) \delta(\sigma_1, -\sigma'_1) \cdots \delta(\sigma_{N-1}, -\sigma'_{N-1}), \quad (2.8)$$

it also commutes with $\mathbf{U}(u)$

$$[\mathbf{U}(u), \mathbf{R}] = 0. \quad (2.9)$$

For simplicity, we suppose that N is an even number. It follows that $\Lambda(u)$ is a doubly periodic function of u :

$$\Lambda(u + 2I') = r\Lambda(u) \quad \text{and} \quad \Lambda(u - 2iI) = \Lambda(u) \times \begin{cases} r & \text{for } T > T_C, \\ 1 & \text{for } T < T_C, \end{cases} \quad (2.10)$$

where r ($= \pm 1$) is the eigenvalue of \mathbf{R} corresponding to $\Lambda(u)$. In addition, it is found that

$$\Lambda(u)\Lambda(u + I') = (-2)^N \times \begin{cases} \frac{1}{\text{sn}(iu)^N} + [\text{ksn}(iu)]^N r & \text{for } T > T_C, \\ \frac{1}{[\text{ksn}(iu)]^N} + \text{sn}(iu)^N r & \text{for } T < T_C. \end{cases} \quad (2.12)$$

We can use (2.12) and (2.13) with the periodicity (2.10) and (2.11) to determine explicit forms of $\Lambda(u)$. For example, it is shown that the maximum eigenvalue $\Lambda_0(u)^2$ behaves as $\Lambda_0(u)^2 \sim \kappa(u)^{2N}$, when N becomes large, and the per-site free energy f is given by

$$-\frac{f}{k_B T} = \ln \kappa(u) = \frac{1}{2\pi} \int_0^\pi d\theta \ln \{2 [\cosh 2K \cosh 2K' + c(\theta)]\}, \quad (2.14)$$

where

$$c(\theta) = (1 - 2k^{-1} \cos 2\theta + k^{-2})^{\frac{1}{2}} \times \begin{cases} k & \text{for } T > T_C, \\ 1 & \text{for } T < T_C \end{cases} \quad (2.15)$$

$$(2.16)$$

(see section 7.9 of [11]).

2.2. Exact analysis: shift operator method

We investigate the correlation function with the help of the shift operator [22, 32]. Choose a site on the sublattice containing the origin \mathbf{o} , whose position vector is denoted by \mathbf{r}^+ . The expectation value of the spin product $\sigma_{\mathbf{o}}\sigma_{\mathbf{r}^+}$ is represented in the usual transfer matrix method as

$$\langle \sigma_{\mathbf{o}}\sigma_{\mathbf{r}^+} \rangle = \frac{\text{Tr}[\mathbf{A}_0 \mathbf{U}^m \mathbf{A}_n \mathbf{U}^{M-m}]}{\text{Tr} \mathbf{U}^M}, \quad \mathbf{r}^+ = n(\mathbf{e}_x + \mathbf{e}_y) + m(-\mathbf{e}_x + \mathbf{e}_y) \quad (2.17)$$

where \mathbf{A}_n is a spin operator defined by the diagonal matrix

$$[\mathbf{A}_n]_{\sigma,\sigma'} = \begin{cases} \sigma_n & \text{for } \sigma = \sigma', \\ 0 & \text{otherwise.} \end{cases} \quad (2.18)$$

In (2.17) we start with choosing two sites on the same sublattice of Λ_{sq} , but this restriction will be removed later.

Applying a similarity transformation to diagonalize \mathbf{U} , we take the $M \rightarrow \infty$ limit first, then the $N \rightarrow \infty$ limit. In the $M \rightarrow \infty$ limit, we find that

$$\langle \sigma_{\mathbf{o}} \sigma_{\mathbf{r}+} \rangle = \sum_p [\tilde{\mathbf{A}}_0]_{0,p} [\tilde{\mathbf{A}}_n]_{p,0} \left[\frac{\Lambda_p(u)}{\Lambda_0(u)} \right]^{2m}, \quad (2.19)$$

where $\Lambda_p(u)^2$ is the p -th eigenvalue of $\mathbf{U}(u)$ in decreasing order of magnitude, and $\tilde{\mathbf{A}}_n$ is the matrix transformed from \mathbf{A}_n . Equation (2.19) implies that the ratios between the eigenvalues essentially determine the asymptotic behavior of the correlation function along the diagonal direction. For example, when n is fixed and m becomes large, the correlation length along the diagonal direction is calculated from the ratios between $\Lambda_0(u)^2$ and the next-largest eigenvalues.

To find the asymptotic form in all directions, we consider the ACL, which is obtainable by taking the $m \rightarrow \infty$ limit with the ratio

$$\gamma = -\frac{n}{m} \quad (2.20)$$

fixed. In this limit, contribution from the matrix elements $[\tilde{\mathbf{A}}_0]_{0,p}$ and $[\tilde{\mathbf{A}}_n]_{p,0}$ is important as well as the ratios between eigenvalues. This causes a difficulty because the direct calculation of the matrix elements is, in most cases, very complicated. However, we can overcome this problem by introducing the shift operator \mathbf{S} [22, 32], which is defined by the matrix with elements

$$[\mathbf{S}]_{\sigma,\sigma'} = \delta(\sigma_0, \sigma'_1) \delta(\sigma_1, \sigma'_2) \cdots \delta(\sigma_{N-1}, \sigma'_0). \quad (2.21)$$

Because the shift operator relates \mathbf{A}_n to \mathbf{A}_0 as

$$\mathbf{A}_n = \mathbf{S}^{-n} \mathbf{A}_0 \mathbf{S}^n, \quad (2.22)$$

it follows from (2.19) that

$$\langle \sigma_{\mathbf{o}} \sigma_{\mathbf{r}+} \rangle = \sum_p [\tilde{\mathbf{A}}_0]_{0,p} [\tilde{\mathbf{A}}_0]_{p,0} \left[\frac{\Lambda_p(u)}{\Lambda_0(u)} \left(\frac{S_p}{S_0} \right)^{\frac{\gamma}{2}} \right]^{2m}, \quad (2.23)$$

where S_p is the p -th eigenvalue of \mathbf{S} and $S_0 = 1$. Equation (2.23) shows that we can obtain the ACL from both the eigenvalues of $\mathbf{U}(u)$ and those of \mathbf{S} without calculating the matrix elements. To consider the $N \rightarrow \infty$ limit, we define limiting functions as

$$L_p(u) = \lim_{N \rightarrow \infty} \frac{\Lambda_p(u)}{\kappa(u)^N}, \quad p = 0, 1, \dots, \quad (2.24)$$

where $\kappa(u)$ is given by (2.14), (2.15) and (2.16); note that $L_0(u) \equiv 1$. It is shown that

$$\frac{S_p}{S_0} = \lim_{u \rightarrow 0} L_p(u)^2. \quad (2.25)$$

From (2.23), (2.24) and (2.25), we obtain

$$\langle \sigma_{\mathbf{o}} \sigma_{\mathbf{r}+} \rangle = \sum_p [\tilde{\mathbf{A}}_0]_{0,p} [\tilde{\mathbf{A}}_0]_{p,0} [L_p(u) L_p(0) \gamma]^{2m}. \quad (2.26)$$

It follows from (2.10)-(2.16) that the limiting function must be of the form

$$L(u) = \pm \prod_{l=1}^{\nu} k^{\frac{1}{2}} \text{sn}(iu - \phi_l - \frac{iI'}{2}), \quad -\frac{I'}{2} < \Re(u) \leq \frac{3I'}{2}, \quad (2.27)$$

where $L(u)$ is labeled by an integer ν and real numbers $\phi_1, \phi_2, \dots, \phi_{\nu}$ instead of p (see Appendix A). For simplicity, we choose the positive sign in (2.27). Detailed analysis shows that the maximum eigenvalue $\Lambda_0(u)^2$ corresponds to the case $r_0 = +1$, and $[\tilde{\mathbf{A}}_0]_{0,p}$ and $[\tilde{\mathbf{A}}_0]_{p,0}$ vanish unless $r_p = -1$, where r_p is the p -th eigenvalue of \mathbf{R} (see section 7.10 of [11]). It is also shown that, because of continuous distributions of eigenvalues, the summation in (2.26) becomes integrals over ϕ_l s in the $N \rightarrow \infty$ limit [36, 37].

For $T > T_C$, only the band of next-largest eigenvalues with $\nu = 1$ and $r = -1$ contributes to the leading asymptotic behavior of the correlation function in the large m limit with γ fixed. It follows that

$$\langle \sigma_{\mathbf{o}} \sigma_{\mathbf{r}+} \rangle - \langle \sigma_{\mathbf{o}} \rangle \langle \sigma_{\mathbf{r}+} \rangle \sim \int_{-I}^I d\phi \rho(\phi) \left\{ k^{\frac{1}{2}} \text{sn}(iu - \phi - \frac{iI'}{2}) \left[k^{\frac{1}{2}} \text{sn}(-\phi - \frac{iI'}{2}) \right]^{\gamma} \right\}^{2m}, \quad (2.28)$$

where the function $\rho(\phi)$ is to be determined from the distribution of eigenvalues, $[\tilde{\mathbf{A}}_0]_{0,p}$, and $[\tilde{\mathbf{A}}_0]_{p,0}$. Note that because $r = +1$ for eigenvalues with $\nu = 2$, $[\tilde{\mathbf{A}}_0]_{0,p}$ and $[\tilde{\mathbf{A}}_0]_{p,0}$ vanish due to the \mathbb{Z}_2 symmetry of the system. Therefore, the first correction to the asymptotic behavior (2.28) comes from an integral over the band of eigenvalues with $\nu = 3$ and $r = -1$ [33, 34].

As stated, we extend the above analysis to include any pair of sites on Λ_{sq} . Because $\mathbf{r}^+ = (n-m)\mathbf{e}_x + (n+m)\mathbf{e}_y$ (figure 1(b)), we obtain the transformation of the coordinates

$$i = n - m, \quad j = n + m. \quad (2.29)$$

We can remove the restriction $i \pm j = \text{even}$ in (2.28) to find the correlation function for all $\mathbf{r} \in \Lambda_{\text{sq}}$ as

$$\langle \sigma_{\mathbf{o}} \sigma_{\mathbf{r}} \rangle - \langle \sigma_{\mathbf{o}} \rangle \langle \sigma_{\mathbf{r}} \rangle \sim \int_{-I}^I d\phi \rho(\phi) \left\{ k \text{sn}(iu - \phi - \frac{iI'}{2}) \text{sn}(-\phi + \frac{iI'}{2}) \left[k \text{sn}(iu - \phi + \frac{iI'}{2}) \text{sn}(-\phi + \frac{iI'}{2}) \right]^{\Gamma} \right\}^j, \quad (2.30)$$

where Γ is the ratio given by

$$\Gamma = \frac{i}{j} = \frac{\gamma + 1}{\gamma - 1}. \quad (2.31)$$

The correlation length ξ along the direction Γ is defined by

$$-\frac{1}{\xi} = \lim_{R \rightarrow \infty} \frac{\ln [\langle \sigma_{\mathbf{o}} \sigma_{\mathbf{r}} \rangle - \langle \sigma_{\mathbf{o}} \rangle \langle \sigma_{\mathbf{r}} \rangle]}{R}, \quad R = \sqrt{i^2 + j^2}, \quad (2.32)$$

where the limit is taken with Γ fixed. We regard ξ as a function of θ , which is the angle between the \mathbf{e}_x direction along which nearest-neighbor spins are coupled by J and the direction Γ [see figure 1(b)]. Explicitly, Γ is related to θ as

$$\Gamma = \frac{1}{\tan \theta}, \quad \frac{\pi}{4} < \theta < \frac{5\pi}{4}. \quad (2.33)$$

We assume an analyticity of $\rho(\phi)$, and then estimate the integral on the right hand side (rhs) of (2.30) by the method of steepest descent. It follows that

$$\begin{aligned} -\frac{1}{\xi} &= \sin \theta \ln \left| k \operatorname{sn}(iu - \phi_s - \frac{iI'}{2}) \operatorname{sn}(-\phi_s + \frac{iI'}{2}) \right| \\ &\quad + \cos \theta \ln \left| k \operatorname{sn}(iu - \phi_s + \frac{iI'}{2}) \operatorname{sn}(-\phi_s + \frac{iI'}{2}) \right|, \end{aligned} \quad (2.34)$$

where the saddle point ϕ_s is determined as a function of θ by

$$\begin{aligned} 0 &= \sin \theta \frac{d}{d\phi_s} \ln \left[k \operatorname{sn}(iu - \phi_s - \frac{iI'}{2}) \operatorname{sn}(-\phi_s + \frac{iI'}{2}) \right] \\ &\quad + \cos \theta \frac{d}{d\phi_s} \ln \left[k \operatorname{sn}(iu - \phi_s + \frac{iI'}{2}) \operatorname{sn}(-\phi_s + \frac{iI'}{2}) \right] \end{aligned} \quad (2.35)$$

with the condition $\phi_s = iu - iI'/2 \pm I$ for $\theta = 3\pi/4$. It follows from the relation $\xi(\theta + \pi) = \xi(\theta)$ that (2.34)-(2.35) is analytically continued into $0 < \theta < 2\pi$.

Note that increasing θ by 2π causes ϕ_s to decrease by $2I'$. We expect that $\rho(\phi)$ is a doubly periodic function, and is analytic inside and on a periodic rectangle. According to Liouville's theorem, it should be a constant. We can rewrite (2.30) as

$$\begin{aligned} \langle \sigma_{\mathbf{o}} \sigma_{\mathbf{r}} \rangle - \langle \sigma_{\mathbf{o}} \rangle \langle \sigma_{\mathbf{r}} \rangle &\sim \\ \text{Const.} \oint \frac{d\alpha}{\alpha} \oint \frac{d\beta}{\beta} \frac{\alpha^i \beta^j}{2a - \gamma_1(\alpha + \alpha^{-1}) - \gamma_2(\beta + \beta^{-1})}, \end{aligned} \quad (2.36)$$

where the contours of the integration are the unit circles, and

$$a = (1 + z_1^2)(1 + z_2^2), \quad \gamma_1 = 2z_2(1 - z_1^2), \quad \gamma_2 = 2z_1(1 - z_2^2) \quad (2.37)$$

with $z_1 = \tanh K$, $z_2 = \tanh K'$. We note that (2.36)-(2.37) is essentially the same as the asymptotic form calculated in section XII-4 of [30] and in section 4 of [31]. In the case of the isotropic interactions the denominator of the integrand possesses the same form as that in a special case of the lhs of (1.3). It follows that the asymptotic correlation function is represented using differential forms on the algebraic curve (1.3).

For $T < T_C$, because the band of next-largest eigenvalues with $\nu = 2$ and $r = -1$ determines the leading asymptotic behavior of the correlation function (see Appendix A), we obtain

$$\begin{aligned} \langle \sigma_{\mathbf{o}} \sigma_{\mathbf{r}+} \rangle - \langle \sigma_{\mathbf{o}} \rangle \langle \sigma_{\mathbf{r}+} \rangle &\sim \\ \int_{-I}^I d\phi_1 \int_{-I}^I d\phi_2 \rho(\phi_1, \phi_2) &\left\{ k^{\frac{1}{2}} \operatorname{sn}(iu - \phi_1 - \frac{iI'}{2}) \left[k^{\frac{1}{2}} \operatorname{sn}(-\phi_1 - \frac{iI'}{2}) \right]^{\gamma} \right\}^{2m} \\ &\times \left\{ k^{\frac{1}{2}} \operatorname{sn}(iu - \phi_2 - \frac{iI'}{2}) \left[k^{\frac{1}{2}} \operatorname{sn}(-\phi_2 - \frac{iI'}{2}) \right]^{\gamma} \right\}^{2m}. \end{aligned} \quad (2.38)$$

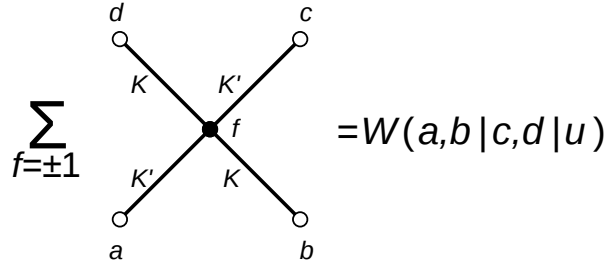


Figure 2. Boltzmann weight of four edges $W(a, b | c, d | u)$, where a , b , c , and d are the nearest-neighbor spins of f to be summed.

Again, the function $\rho(\phi_1, \phi_2)$ is to be calculated from the distribution of eigenvalues, $[\tilde{\mathbf{A}}_0]_{0,p}$, and $[\tilde{\mathbf{A}}_0]_{p,0}$. Assume an analyticity of $\rho(\phi_1, \phi_2)$, and integrate by steepest descents. Then, we find that the correlation length ξ^* below T_C is related to ξ above T_C determined by (2.34)-(2.35) as

$$\xi = 2\xi^* \quad (2.39)$$

for all directions. We also find that (2.38) is essentially the same asymptotic form as in section XII-3 of [30] and in section 3 of [31].

2.3. Exact analysis: passive rotation

The method in section 2.2 corresponds to the active rotations. To find a role of the C_{4v} (or C_{2v}) symmetry, we consider the passive rotations: We define the Ising model on a square lattice rotated through an arbitrary angle with respect to the coordinate axes. The rotated system is related to an inhomogeneous system possessing a one-parameter family of commuting transfer matrices. A product of commuting transfer matrices can be interpreted as a transfer matrix acting on zigzag walls in the rotated system [21, 38].

For convenience, we denote the Boltzmann weight of four edges as

$$W(a, b | c, d | u) = 2 \cosh(K'a + Kb + K'c + Kd), \quad (2.40)$$

where a , b , c , and d are the nearest-neighbor spins of f arranged as in figure 2. Note that K , K' are given by (2.5) for $T > T_C$ and by (2.6) for $T < T_C$. The weight $W(a, b | c, d | u)$ satisfies the following properties [38], i.e., the standard initial condition

$$\lim_{u \rightarrow 0} \frac{W(a, b | c, d | u)}{\kappa(u)^2} = \delta(a, c), \quad (2.41)$$

and the crossing symmetry condition

$$W(a, b | c, d | I' - u) = W(b, a | d, c | u), \quad (2.42)$$

where $\kappa(u)$ is given by (2.14), (2.15) and (2.16). Since $\kappa(I' - u) = \kappa(u)$, it follows from (2.41) and (2.42) that

$$\lim_{u \rightarrow I'} \frac{W(a, b | c, d | u)}{\kappa(u)^2} = \delta(b, d). \quad (2.43)$$

To analyze a square lattice rotated through an arbitrary angle θ , we consider inhomogeneous transfer matrices. Let $\sigma = \{\sigma_0, \sigma_1, \dots, \sigma_{N-1}\}$ (respectively $\sigma' = \{\sigma'_0, \sigma'_1, \dots, \sigma'_{N-1}\}$) be the spins on the lower (respectively upper) row of open circles shown in figure 1(a). Further, suppose that $N = (|n| + m)N_0$, where $m > 0$ and N_0 is an even number. Then, we can define inhomogeneous transfer matrices as

$$\begin{aligned} [\mathbf{U}_{\text{IH}}(u)]_{\sigma, \sigma'} &= \prod_{l=0}^{N_0-1} \left[\prod_{s=l(|n|+m)}^{l(|n|+m)+|n|-1} W(\sigma_s, \sigma_{s+1} | \sigma'_{s+1}, \sigma'_s | u) \right. \\ &\quad \left. \times \prod_{t=l(|n|+m)+|n|}^{(l+1)(|n|+m)-1} W(\sigma_t, \sigma_{t+1} | \sigma'_{t+1}, \sigma'_t | u + u_0 - H(-n)I') \right], \end{aligned} \quad (2.44)$$

where $\sigma_N = \sigma_0$ and $\sigma'_N = \sigma'_0$, and $H(\cdot)$ is the Heaviside step function. Similarly to the uniform case (2.7) and (2.8), $\mathbf{U}_{\text{IH}}(u)$ commutes with each other

$$[\mathbf{U}_{\text{IH}}(u), \mathbf{U}_{\text{IH}}(u')] = 0 \quad \forall u, u' \in \mathbb{C}, \quad (2.45)$$

and with the spin reversal operator

$$[\mathbf{U}_{\text{IH}}(u), \mathbf{R}] = 0. \quad (2.46)$$

By using $\mathbf{U}_{\text{IH}}(u)$, we can construct a transfer matrix $\bar{\mathbf{U}}$ acting on zigzag walls in the rotated system as

$$\bar{\mathbf{U}} = \begin{cases} \left[\lim_{u \rightarrow 0} \frac{\mathbf{U}_{\text{IH}}(u)}{\kappa(u)^{2|n|N_0}} \right]^m \left[\lim_{u \rightarrow I' - u_0} \frac{\mathbf{U}_{\text{IH}}(u)}{\kappa(u + u_0)^{2mN_0}} \right]^{|n|} & \text{for } n > 0, \\ \left[\lim_{u \rightarrow I'} \frac{\mathbf{U}_{\text{IH}}(u)}{\kappa(u)^{2|n|N_0}} \right]^m \left[\lim_{u \rightarrow I' - u_0} \frac{\mathbf{U}_{\text{IH}}(u)}{\kappa(u + u_0 - I')^{2mN_0}} \right]^{|n|} & \text{for } n \leq 0, \end{cases} \quad (2.47)$$

where n and m are related to θ by $-n/m = \tan(\theta + \pi/4)$ with $\pi/4 < \theta < 5\pi/4$ (see figure 2 of [38]). $\bar{\mathbf{U}}$ reduces to the row-to-row transfer matrix in the case $n = m$ (or $n = -m$), and to the diagonal-to-diagonal transfer matrix in the case $n = 0$. We can find the correlation length along any direction of θ from the eigenvalues of $\bar{\mathbf{U}}$.

Noting the relations

$$\begin{aligned} \sum_f W(a, b|f, d|u)W(f, b|c, d| -u) &= -(2 \sinh 2K')^2 \delta(a, c), \\ \sum_f W(a, b|f, d|u - I')W(f, b|c, d| -u + I') &= -(2 \sinh 2K)^2 \delta(a, c), \end{aligned} \quad (2.48)$$

with $\sinh 2K, \sinh 2K'$ given by (2.5) or (2.6), we also construct a shift operator $\bar{\mathbf{S}}$ as

$$\begin{aligned} \bar{\mathbf{S}} &= \left[\lim_{u \rightarrow 0} \frac{\mathbf{U}_{\text{IH}}(u)}{\kappa(u)^{2|n|N_0}} \right]^{|n|} \\ &\quad \times \begin{cases} \left[- \lim_{u \rightarrow -u_0} (2 \sinh 2K')^2 \right]^{-|n|mN_0} \left[\lim_{u \rightarrow -u_0} \frac{\mathbf{U}_{\text{IH}}(u)}{\kappa(u + u_0)^{2mN_0}} \right]^m & \text{for } n > 0, \\ \left[- \lim_{u \rightarrow -u_0} (2 \sinh 2K)^2 \right]^{-|n|mN_0} \left[\lim_{u \rightarrow I' - u_0} \frac{\mathbf{U}_{\text{IH}}(u)}{\kappa(u + u_0 - I')^{2mN_0}} \right]^m & \text{for } n \leq 0. \end{cases} \end{aligned} \quad (2.49)$$

We denote eigenvalues of $\mathbf{U}_{\text{IH}}(u)$ as $\Lambda_{\text{IH}}(u)^2$. When N_0 (or N) becomes large with n and m fixed, the maximum eigenvalue $\Lambda_{\text{IH};0}(u)^2$ behaves as

$$\Lambda_{\text{IH};0}(u)^2 \sim \kappa(u)^{2|n|N_0} \kappa(u + u_0 - H(-n)I')^{2mN_0}, \quad (2.50)$$

where $\kappa(u)$ is given by (2.14), (2.15) and (2.16) [35, 39]. Also, we shall introduce the limiting function as

$$L_{\text{IH}}(u) = \lim_{N_0 \rightarrow \infty} \frac{\Lambda_{\text{IH}}(u)}{\kappa(u)^{2|n|N_0} \kappa(u + u_0 - H(-n)I')^{2mN_0}}. \quad (2.51)$$

The expectation value of the spin product $\sigma_{\mathbf{o}}\sigma_{\mathbf{r}+}$ is represented as

$$\langle \sigma_{\mathbf{o}}\sigma_{\mathbf{r}+} \rangle = \sum_p [\bar{\mathbf{A}}_0]_{0,p} [\bar{\mathbf{A}}_0]_{p,0} L_{\text{IH};p}(-H(-n)I')^{2m} L_{\text{IH};p}(I' - u_0)^{2|n|}, \quad (2.52)$$

where $\bar{\mathbf{A}}_0$ is the matrix transformed from \mathbf{A}_0 in (2.18) by a similarity transformation that diagonalizes $\mathbf{U}_{\text{IH}}(u)$. Almost the same argument as in Appendix A yields that $L_{\text{IH}}(u)$ must be of the form

$$L_{\text{IH}}(u) = \pm \prod_{l=1}^{\nu} k^{\frac{1}{2}} \text{sn}(iu - \bar{\phi}_l - \frac{iI'}{2}), \quad (2.53)$$

where $\bar{\phi}_l$ are complex numbers determined by the condition that the eigenvalues of the shift operator $\bar{\mathbf{S}}$ are unimodular:

$$|L_{\text{IH}}(-u_0)^m L_{\text{IH}}(0)^n| = 1. \quad (2.54)$$

From (2.53) and (2.54), we can reproduce the asymptotic behavior of the correlation function found in section 2.2: (2.28) or (2.30) for $T > T_C$, and (2.38) for $T < T_C$.

Now, we consider the correlation function for $T > T_C$ (almost the same argument holds for $T < T_C$). The asymptotic correlation function is given as follows:

$$\langle \sigma_{\mathbf{o}}\sigma_{\mathbf{r}+} \rangle - \langle \sigma_{\mathbf{o}} \rangle \langle \sigma_{\mathbf{r}+} \rangle \sim \int_C d\bar{\phi} \bar{\rho}(\bar{\phi}) \left[k^{\frac{1}{2}} \text{sn}(-\bar{\phi} - \frac{iI'}{2}) \right]^{2m} \left[k^{\frac{1}{2}} \text{sn}(-iu_0 - \bar{\phi} + \frac{iI'}{2}) \right]^{2n}. \quad (2.55)$$

Note that the contour C is determined by the condition (2.54), and the rotations of the lattice deform C . For instance, in the case $n = 0$ ($\theta = 3\pi/4$), \int_C denotes an integral over a period interval of the length $2I$ on the line $\Im[\bar{\phi}] = -u_0$, where (2.55) reduces to (2.28) by the relations $\bar{\phi} = \phi - iu_0$ and $\bar{\rho}(\bar{\phi}) = \rho(\phi)$ with u_0 replaced by u . In the case $n = m$ ($\theta = \pi/2$), the contour C is on the line $\Im[\bar{\phi}] = -u_0/2$, where the equivalence of (2.28) and (2.55) is derived with the help of the analyticity of the integrand.

2.4. Structure of elliptic curve in asymptotic correlation function

To show a role of the C_{4v} (or C_{2v}) symmetry, we compare the method in section 2.3 with that in section 2.2. We cannot directly relate $\bar{\mathbf{U}}$ to the diagonal-to-diagonal transfer matrix \mathbf{U} in section 2.1 and section 2.2. However, as we observed above, after the eigenvalues are summed up, the results of $\bar{\mathbf{U}}$ are equivalent to those of \mathbf{U} . This equivalence is derived using analytic properties of the integrands in (2.28) and (2.55).

Therefore, (i) analyticity of $L_{\text{IH}}(u)$ [and $L(u)$ in section 2.2] is needed to ensure the equivalence between the methods in section 2.2 and section 2.3.

Two further properties are pointed out: We find that decreasing θ by π causes C to shift by I' along the imaginary axis. It follows that (ii) the inversion symmetry is directly connected with the inversion relation

$$L_{\text{IH}}(u + I') = L_{\text{IH}}(u)^{-1}, \quad (2.56)$$

which corresponds to the first equation of (A.1) or (A.2). Because the second equation of (A.1) or (A.2) is also satisfied by $L_{\text{IH}}(u)$, it follows that $L_{\text{IH}}(u)$ is a doubly periodic function. Note that (1.2) and (1.3) represent elliptic curves (i.e., they are algebraic curves of genus 1) [40]. From (2.28), (2.36) and (2.55), we find that (iii) the asymptotic correlation function is written in terms of elliptic functions (or differential forms on a Riemann surface of genus 1).

The meaning of (iii) can be explained as follows: 2D lattice models are related to 2D Euclidean field theories in the critical limit and for distances much larger than the lattice spacing. For a Euclidean field, the dispersion relation is written as $p_x^2 + p_y^2 + m^2 = 0$ with a suitable mass term m , and the correlation function has a periodic structure describing the rotational symmetry. For off-critical lattice models, two kinds of periodicity appear: one is connected with two-, four-, or six-fold rotational symmetry, and the other with the fact that eigenvalues of the transfer matrix are periodic functions of crystal momentum. This doubly periodic structure leads to the property (iii).

We would like to stress that (i)~(iii) are quite general properties satisfied by a wide class of lattice models. Using them, we can essentially determine the form of $L_{\text{IH}}(u)$ and the asymptotic behavior of the correlation functions. The property (iii) shows that, choosing a suitable parameterization, we can write the correlation function as

$$\langle \sigma_{\mathbf{o}} \sigma_{\mathbf{r}} \rangle - \langle \sigma_{\mathbf{o}} \rangle \langle \sigma_{\mathbf{r}} \rangle \sim \int_{-\omega_1}^{\omega_1} d\Theta \mathcal{Y}(\Theta)^j \mathcal{X}(\Theta)^i, \quad (2.57)$$

where $\mathcal{Y}(\Theta)$ comes from eigenvalues of the row-to-row transfer matrix, and $\mathcal{X}(\Theta)$ the corresponding ones of the shift operator; $\mathcal{X}(\Theta)$ and $\mathcal{Y}(\Theta)$ are doubly periodic: $\mathcal{X}(\Theta + 2\omega_1) = \mathcal{X}(\Theta + 2\omega_2) = \mathcal{X}(\Theta)$ and $\mathcal{Y}(\Theta + 2\omega_1) = \mathcal{Y}(\Theta + 2\omega_2) = \mathcal{Y}(\Theta)$. The property (ii) yields the inversion relations $\mathcal{Y}(\Theta + \omega_2) = \mathcal{Y}(\Theta)^{-1}$ and $\mathcal{X}(\Theta + \omega_2) = \mathcal{X}(\Theta)^{-1}$, and the property (i) indicates analyticity of $\mathcal{Y}(\Theta)$ and $\mathcal{X}(\Theta)$. As a result, $\mathcal{Y}(\Theta)$ and $\mathcal{X}(\Theta)$ must be of the forms

$$\mathcal{Y}(\Theta) = \prod_{l=1}^{\mu} ik^{\frac{1}{2}} \text{sn}(\Theta + \alpha_l), \quad \mathcal{X}(\Theta) = \prod_{l=1}^{\mu'} ik^{\frac{1}{2}} \text{sn}(\Theta + v + \beta_l). \quad (2.58)$$

The present square-lattice Ising model possesses the C_{2v} symmetry. It is shown that $v = \pm\omega_2/2$, and further in the isotropic case $K = K'$ ($J = J'$), $\mu = \mu'$ and $\alpha_l = \beta_l$ owing to the C_{4v} symmetry of the system. From the correlation function being real-valued, we find that the modular parameter $\tau = \omega_2/\omega_1$ must be pure imaginary. It follows from (2.30) that the simplest case $\mu = 2$ appears for $T > T_C$. For parameters α_1 and α_2 , we find two possibilities: $(\alpha_1 - \alpha_2)/\omega_1$ is pure-imaginary or a real number;

$\alpha_1 - \alpha_2 = \omega_2/2$ gives (2.30), which is rewritten as (2.36). The structure of the elliptic curve in its integrand is closely related to the C_{4v} (or C_{2v}) symmetry, and thus expected to be a quite general consequence.

Almost the same argument holds for $T < T_C$: Equation (2.38) shows that $\mu = 4$, and that $\alpha_1 - \alpha_2 = \alpha_3 - \alpha_4 = \omega_2/2$, and $\alpha_1 - \alpha_3$ is a real number. The only difference from the case of $T > T_C$ is that two elliptic curves are needed to represent the asymptotic correlation function (see section XII-3 of [30] and section 3 of [31]).

3. Numerical analysis and universal form for asymptotic correlation functions

As discussed in section 2.4, the structure of the elliptic curve in (2.36) is expected to appear for general Q . To show this, we numerically investigate the correlation functions and the ACLs. The definition of the correlation function for the Q -state Potts model is

$$\langle \sigma_{\mathbf{o}} \sigma_{\mathbf{r}} \rangle = \left\langle \frac{Q\delta(q_{\mathbf{o}}, q_{\mathbf{r}}) - 1}{Q - 1} \right\rangle = \left\langle \exp \left[\frac{2\pi i(q_{\mathbf{o}} - q_{\mathbf{r}})}{Q} \right] \right\rangle, \quad (3.1)$$

which coincides with that for $Q = 2$ and $T > T_C$ in section 2. It was rigorously proven that the correlation function decays exponentially above the transition temperature and at the first-order transition point [12, 17, 41]. For the latter some authors calculated the correlation lengths exactly [8, 14, 15].

Numerical calculations of the correlation functions and the correlation lengths have been also frequently performed. One typical way of doing them is to analyze the exponential decay of correlation function data in a certain fixed direction provided by MC simulation calculations on finite systems [42, 43]. However, it is recognized that such an approach cannot always give an accurate estimation of the correlation lengths. Further, if we use a similar approach to the above, our analysis on the ACLs is naturally expected to become more difficult because of the following reasons: First, the finite-size effects in the MC data can affect the analysis of anisotropy in an unexpected manner. Second, because the patterns of the ACLs observed in different models, but sharing the same lattice symmetry, are similar to each other [44, 45], they may give only weak signals of their differences (see also Appendix B).

In this situation, as the MC method, we employ a cluster algorithm proposed by Evertz and von der Linden [46], which is called infinite-system method since an extrapolation of data to the thermodynamic limit is not necessary. For a system in a disordered phase, we generate the random clusters by taking the center site as a seed site, and expand the thermally equilibrated area outward (for details, see Appendix B). Then, we measure the correlation functions in the area well equilibrated, which are free of the finite-size effects. Typically $O(10^{14})$ random clusters are generated at each temperature to attain the high accuracy of MC data [29]. We propose a combined use of the MC data with the result in section 2.4, which is quite efficient to investigate the ACLs.

In section 3.1, we shall introduce a form for asymptotic correlation functions which includes three parameters. To determine them, fitting calculations are performed for the MC data. In section 3.2, we calculate the ACL in the $Q = 2$ Potts model to demonstrate an accuracy of our numerical analysis. In section 3.3, we investigate the structure of the algebraic curve for $Q = 3, 4$. In section 3.4 we also apply the method to the bond percolation process corresponding to the $Q \rightarrow 1$ limit.

3.1. Universal form for asymptotic correlation functions in the Q -state Potts model

Based on the observation in section 2, we shall propose a universal form for asymptotic behavior of correlation functions. In what follows, we concentrate on the isotropic case $J_{\mathbf{r},\mathbf{r}'} = 2J$, where the transition point is simply given by $k_{\text{B}}T_{\text{C}}(Q)/J = 2/\ln(1 + \sqrt{Q})$. For $T > T_{\text{C}}(Q)$, the C_{4v} lattice symmetry permits the inclusion of one fitting parameter other than the elliptic modulus and a normalization factor because it does not impose the condition $\alpha_1 - \alpha_2 = \omega_2/2$ (see section 2.4): In terms of elliptic functions, our form is expressed as

$$\mathcal{F}_{\text{sq}}(i, j; A, k, b) = \frac{A}{\pi}(1 - k^2)^{\frac{1}{4}} \times \int_{-I}^I d\phi \left[k \text{sn}\left(\phi + b\frac{iI'}{4}\right) \text{sn}\left(\phi - b\frac{iI'}{4}\right) \right]^j \left[k \text{sn}\left(\phi + (2+b)\frac{iI'}{4}\right) \text{sn}\left(\phi + (2-b)\frac{iI'}{4}\right) \right]^i. \quad (3.2)$$

Besides the modulus k and the normalization factor A , we introduced b as a fitting parameter. We take the Ising model as a reference, i.e., A and b may, respectively, refer to the exact values $A = 1$ and $b = 1$ in the $Q = 2$ case. Further, k can be related to the inverse correlation length in the diagonal direction as

$$\frac{1}{\xi_{\text{diag}}} = -\frac{1}{\sqrt{2}} \ln k, \quad (3.3)$$

which is exact for the Ising model.

We denote MC data of (3.1) with $\mathbf{r} = i\mathbf{e}_x + j\mathbf{e}_y \in \Lambda_{\text{sq}}$ by $\{c(i, j)\}$. In an asymptotic region of large R , we perform a fitting of MC data to determine the three parameters A, k, b . Using the extracted values $\bar{A}, \bar{k}, \bar{b}$, the asymptotic correlation function is represented as

$$\langle \sigma_{\mathbf{o}} \sigma_{\mathbf{r}} \rangle \sim \mathcal{F}_{\text{sq}}(i, j; \bar{A}, \bar{k}, \bar{b}) \quad \text{for large } \mathbf{r}. \quad (3.4)$$

We can find the ACL from (3.4) by the method of steepest descent, as shown in section 2.2. If we succeed in calculating the ACL with a sufficient accuracy, it gives strong numerical evidence that the same structure of the elliptic curve as that in (2.36) appears in the asymptotic correlation function.

To optimize an accuracy of our numerical analysis, we need to carefully choose a fitting region of the MC data. There are two possible sources of errors in our analysis: One is the statistical errors in $\{c(i, j)\}$, which are inherent in the MC sampling procedures, and the other is systematic errors in (3.2). Note that, a contribution from higher bands of eigenvalues is not taken into account in (3.2) though it is important for

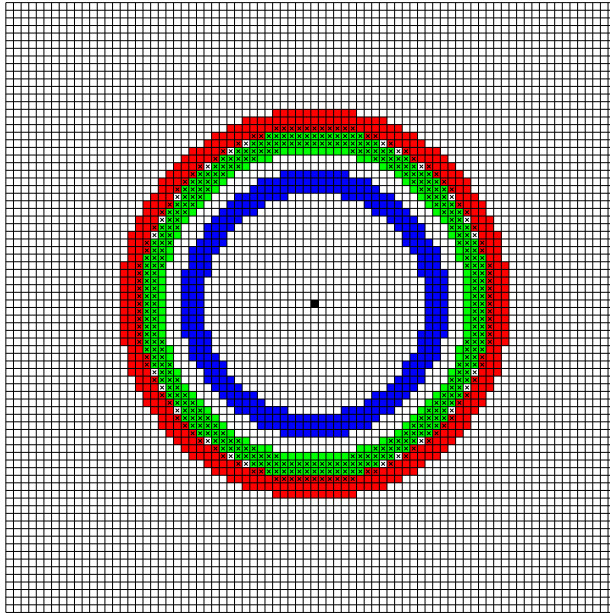


Figure 3. Examples of annular regions. The origin $(0, 0)$ is denoted by the black cell. The annular region $\mathcal{D}(10^{-3}, 3 \times 10^{-4})$ is employed for the fitting of correlation function data of $Q = 2$ at $t = 0.24$ (308 blue cells). The annulus for $Q = 3$ at $t = 0.15$ and that for $Q = 4$ at $t = 0.1$ are indicated by green cells and red cells, respectively. The annulus for $Q = 1$ at $t = 0.50$ are given by crosses overwritten on the cells.

short distances. In general, although an accuracy of shorter-distance MC data is higher than that of longer-distances ones, the fitting results for the shorter can become worse owing to the systematic errors. Meanwhile, for the analysis of ACLs, it is natural to fit the MC data in an annular region instead of those in a fixed direction. We find that by optimizing a mean radius of the annular region, we can obtain reliable fitting results under a well-controlled condition of two kinds of errors. For details of our fittings, see below and Appendix C.

3.2. $Q = 2$ case

We start with the $Q = 2$ Potts model, and demonstrate an accuracy of our numerical analysis. We performed intensive MC simulations to achieve a demanded accuracy and fitting the MC data in a suitable annular region. To make it explicit, let us denote an annular region centered at the origin as $\mathcal{D}(c_{\max}, c_{\min}) = \{(i, j) | c_{\min} < c(i, j) < c_{\max}\}$, and the number of included sites as $|\mathcal{D}(c_{\max}, c_{\min})|$. For instance, at the reduced temperature $t = [T - T_C(2)]/T_C(2) = 0.24$, we employed $|\mathcal{D}(10^{-3}, 3 \times 10^{-4})| = 308$ with a mean radius $\simeq 16$, as given by blue cells in figure 3. The second part of table 1 summarizes the results of $Q = 2$. Then, one can find that, at all temperatures t , our results coincide with the exact Ising values, $\xi_{\text{diag}} = \xi_{\text{exact}}$, $A = 1$ and $b = 1$ within, at least, five-digit accuracy.

As explained in section 2.2, the systematic errors for the $Q = 2$ Potts model stem

Table 1. The temperature dependence of extracted values of the fitting parameters in (3.2). In addition, the correlation length ξ_{diag} is enumerated; its exact values are given in the $Q = 2$ case for comparison. The parenthesized digits include errors. The geometries of annular regions employed for fittings are summarized (see text).

Q	t	c_{max}	c_{min}	$ \mathcal{D} $	A	k	b	ξ_{diag}	ξ_{exact}
1	0.50	1×10^{-4}	3×10^{-5}	436	1.0248(2)	0.59350(7)	1.0184(0)	2.75057(0)	n/a
	0.65	1×10^{-4}	3×10^{-5}	252	1.01859(7)	0.50773(0)	1.0163(4)	2.11350(2)	
	1.00	1×10^{-4}	1×10^{-5}	252	1.01073(6)	0.365456	1.01229(2)	1.418421	
	1.50	1×10^{-3}	1×10^{-4}	104	1.00563(7)	0.245846	1.00872(7)	1.01468(8)	
	2.00	1×10^{-3}	1×10^{-4}	68	1.00330(5)	0.176466	1.006455	0.819235	
	3.00	1×10^{-3}	1×10^{-4}	44	1.0013(5)	0.103562	1.00390(1)	0.625435	
	5.00	1×10^{-2}	1×10^{-4}	36	1.00054(6)	0.048141(9)	1.001795	0.466765	
14.00	1×10^{-2}	1×10^{-5}	32	1.00003(5)	0.0081734(7)	1.000275	0.294259		
2	0.24	1×10^{-3}	3×10^{-4}	308	1.00000(6)	0.59624(2)	0.99998(7)	2.73482(3)	2.734823
	0.30	1×10^{-2}	1×10^{-3}	272	1.00000(0)	0.534544	1.00000(6)	2.25790(6)	2.257906
	0.50	1×10^{-2}	1×10^{-3}	132	0.99999(8)	0.386861	1.000001	1.489133	1.489133
	1.00	1×10^{-2}	1×10^{-3}	52	0.99999(6)	0.207107	1.00000(1)	0.89818(8)	0.898187
	2.00	1×10^{-1}	1×10^{-3}	32	1.000001	0.088825(3)	1.000000	0.584124	0.584124
	10.00	1×10^{-1}	1×10^{-4}	20	0.99999(9)	0.0064337(4)	1.000000	0.280253	0.280253
3	0.15	1×10^{-4}	3×10^{-5}	400	0.9685(6)	0.5927(1)	0.9851(4)	2.67297(9)	n/a
	0.20	1×10^{-4}	3×10^{-5}	280	0.97481(1)	0.52116(8)	0.9862(4)	2.14720(9)	
	0.30	1×10^{-4}	1×10^{-5}	284	0.98281(5)	0.41484(1)	0.9881(3)	1.59277(2)	
	0.50	1×10^{-4}	1×10^{-5}	152	0.9907(2)	0.28411(6)	0.99103(1)	1.11624(3)	
	1.00	1×10^{-3}	1×10^{-4}	48	0.99683(2)	0.141663	0.99507(9)	0.721034(6)	
	2.00	1×10^{-3}	1×10^{-5}	60	0.9992(3)	0.057265(5)	0.997884	0.49373(9)	
	8.00	1×10^{-2}	1×10^{-5}	24	0.99997(7)	0.0057675(6)	0.999812	0.274278(7)	
4	0.10	3×10^{-5}	1×10^{-5}	428	0.93099(3)	0.5983(6)	0.9718(9)	2.69525(2)	n/a
	0.14	3×10^{-5}	1×10^{-5}	264	0.9451(6)	0.52232(4)	0.9742(4)	2.1351(1)	
	0.20	1×10^{-4}	1×10^{-5}	332	0.9591(7)	0.43645(7)	0.97709(0)	1.6763(2)	
	0.30	1×10^{-4}	1×10^{-5}	204	0.9730(8)	0.33772(6)	0.98076(5)	1.2839(9)	
	0.50	1×10^{-4}	1×10^{-5}	100	0.9860(5)	0.22315(0)	0.9858(0)	0.93294(5)	
	1.00	1×10^{-4}	1×10^{-5}	40	0.9957(0)	0.106277	0.99243(5)	0.62743(9)	
	2.00	1×10^{-3}	1×10^{-5}	48	0.99896(8)	0.0413266	0.996967	0.442926(3)	
	6.00	1×10^{-2}	1×10^{-5}	32	0.99993(0)	0.0066875(1)	0.999560	0.282339(6)	

from the third-band eigenvalues, and thus should be smaller than those in other cases. This permits us to use (3.2) for inner annuli. We have checked a very weak dependence of fitting results on radii of inner annuli (see Appendix C). In outer regions the statistical errors become larger. However, we have also checked that their accuracy is improved by increasing the MC steps.

Also, see the second part of table 2; we can confirm that (3.2) is a quite efficient form of the asymptotic correlation functions, especially, to analyze the correlation lengths with their full anisotropies. This is the main advantage in our method over the naive use of the Ornstein-Zernicke form.

3.3. $Q = 3, 4$ cases

In this subsection, we analyze the ACLs observed in the $Q = 3, 4$ Potts models by using the same method as section 3.2. As mentioned, the vanishing of the second-band contribution is due to the \mathbb{Z}_2 symmetry of the $Q = 2$ Potts model, so here we cannot expect the same. In fact, if we compare the $Q = 2$ and $t = 0.24$ case with the $Q = 3$ and $t = 0.15$ case, though ξ_{diag} s are nearly equal to each other (i.e., $\bar{\xi} \simeq 2.7$), we cannot attain the same accuracy of the fitting for the latter MC data in the former annulus (i.e., blue cells in figure 3). We cannot attribute it to the statistical errors, but to an influence from the second-band contributions in the latter. Therefore, to circumvent the systematic errors, we need to employ annuli with larger radii than those in the $Q = 2$ case. For this issue, we estimate the order of errors included in (3.2) to optimize the annulus employed in the $Q = 2$ case. In the $Q = 3$ and $t = 0.15$ case, denote the deviation at the origin $(0, 0)$ as $\Delta(3)$, which is estimated as $\Delta(3) \simeq O(10^{-2})$ (see Appendix C). The systematic error due to the second-band contribution can be calculated as $\Delta(3) \times e^{-2R/\bar{\xi}}$. To obtain the ACL within a sufficient accuracy, we employ $|\mathcal{D}(10^{-4}, 3 \times 10^{-5})| = 400$ with the mean radius $\simeq 21$, which is depicted by the green cells in figure 3. The third part of table 1 summarizes the results for the $Q = 3$ Potts model. We succeeded in fitting the data by (3.2), which permits us to evaluate the ACL of the model within five-digit accuracy at all temperatures calculated. As in the $Q = 2$ case, we checked that the improvement of the accuracy was observed for the fitting of data in the outer annulus by increasing MC steps. The obtained results exhibit the relevant deviation from the Ising values; we will discuss its physical meanings in section 4.

In the $Q = 4$ Potts model, the second-band contributions become somewhat larger than those in the $Q = 3$ case. This can be recognized via the same argument as above: We compare the $Q = 3$ and $t = 0.15$ case with the $Q = 4$ and $t = 0.10$ case; the correlation lengths in these cases are nearly equal. We can also estimate the deviation $\Delta(4)$, and then find that it becomes larger than $\Delta(3)$. Therefore, we should employ a slightly larger annulus in radius than corresponding one in the $Q = 3$ case. Based on the same order-estimate of the second-band contributions as the above, for instance for $t = 0.10$, we employed $|\mathcal{D}(3 \times 10^{-5}, 10^{-5})| = 428$ with mean radius $\simeq 24$, which is indicated by the red cells in figure 3. The fitting can be performed with the same accuracy as in the $Q = 3$ case, and the obtained results are summarized in the fourth part of table 1. As expected, the deviations from the Ising values become more prominent.

3.4. Bond percolation process as $Q \rightarrow 1$ limit

The Potts model is related to a number of other problems in the lattice statistics [11, 12]. These relations make it possible to explore their properties from known results on the Potts model or vice versa [47, 48, 49]. The bond percolation provides a simple picture of a phase transition [50]. Regarding Q as a continuous variable [49], we can relate the Q -state Potts model to the bond percolation model: Suppose that $Z(Q)$ is the partition function of the Q -state Potts model whose cluster representation (B.2) is provided in

Appendix B, then the generating function of the bond percolation is given by

$$\lim_{Q \rightarrow 1} \frac{\partial}{\partial Q} \ln Z(Q), \quad (3.5)$$

where the bond percolation probability is $p = 1 - e^{-2K}$ [11], and the percolation threshold p_C is p at $T_C(1)$. The connectivity function is defined by the probability that the origin \mathbf{o} and the site \mathbf{r} belong to a same cluster, and was proven that, for $p < p_C$, it decays exponentially as \mathbf{r} becomes large [51, 52, 53]. The correlation function (3.1) reduces to the connectivity function in the $Q \rightarrow 1$ limit [12]. Therefore, in this subsection, we investigate the connectivity function in the bond percolation, equivalently the correlation function of the Potts model in the $Q \rightarrow 1$ limit, by using (3.2).

The first part of table 1 summarizes the fitting results for $Q = 1$. Based on the same argument in the above, we optimized the annular regions: for example for $t = 0.50$, we employ $|\mathcal{D}(10^{-4}, 3 \times 10^{-5})| = 436$ with mean radius $\simeq 22$, which is given by crosses in figure 3. Then, we performed the fittings of the MC data in the optimized annuli to determine A , k , b . We obtained the ACL within five-digit accuracy. In the course of fitting calculations, we recognized the systematic errors similarly to the $Q = 3, 4$ cases. The extracted parameter values A and b exhibit deviations from the Ising values in the opposite direction to the $Q = 3, 4$ cases, and reveal their monotonic Q -dependence.

As demonstrated, the form (3.2) can accurately fit the asymptotic correlation functions of the $Q = 2, 3, 4$ Potts models for $T > T_C$, and the asymptotic connectivity function of the bond percolation ($Q = 1$) for $p < p_C$. The result strongly suggests that the same structure of the elliptic curve as that in (2.36) appears for general Q . Consequently, we expect that the structure plays a key role to describe the asymptotic correlation functions in a wide class of models.

4. Discussion and summary

We have investigated the correlation functions of the Q -state Potts model on the square lattice. Revisiting the exact solutions of the Ising model, we found that the asymptotic behavior of the correlation function is expressed in terms of the elliptic functions. In addition, we found the elliptic functions are essentially determined from the C_{4v} (or C_{2v}) lattice symmetry. These properties are expected to be quite general and satisfied by a wide class of lattice models. Based on these observations, we have proposed the new approach to analyze the correlation functions by using the analytical result and the numerical procedures combined: We brought the analytical structure into the form for the asymptotic correlation functions, i.e., (3.2). Because it includes three parameters A , k , b not determined by the lattice symmetry, we performed MC simulations using the infinite-system algorithm [46], then carried out fittings of MC data to determine the parameters.

To demonstrate efficiency of the new approach, we applied it to calculate the ACL of the Ising model ($Q = 2$) for $T > T_C$. As mentioned in section 3, one typical way of calculating the correlation length is to consider the exponential decay of the correlation

function along a fixed direction, but it is difficult to calculate the ACL accurately by this method due to two types of errors: statistical errors and systematic errors. To control the two types of errors, we introduced the annular regions for the fittings, then determined the three parameters. The obtained results agree well with the exact values. To show a wide applicability of (3.2), we investigated the $Q = 3, 4$ Potts models for $T > T_C$ and the bond percolation model (the $Q \rightarrow 1$ limit) for $p < p_C$. Although corrections to (3.2) are somewhat large in these cases, we succeeded in fitting the data within a five-digit accuracy. The results for $Q = 1, 2, 3$, and 4 show the validity of the universal form (3.2), and also the importance of the role of the directional dependence included there, which is the reason for the high accuracy of our approach.

It was revealed that (I) the parameter b monotonically decreases with the increase of Q , and that (II) the Q -state Potts models, including the bond percolation as $Q = 1$, share the same structure of the elliptic curves. It is noticeable that, although small in magnitude, (I) provides the first reliable evidence of a Q -dependence of the ACL. Here, to describe its implication to physics, we investigate the Q -dependence of the ECS. In a previous work [8], we showed that for $Q \geq 2$ the ACL is related to the anisotropic interfacial tension as

$$\frac{\gamma^*}{k_B T^*} = \frac{1}{\xi} \quad \text{for all directions,} \quad (4.1)$$

where γ^* is the anisotropic interfacial tension at a temperature T^* [$< T_C(Q)$] such that $K^* = J/k_B T^*$ satisfies the duality condition $(e^{2K} - 1)(e^{2K^*} - 1) = Q$. γ^* is regarded as a function of θ_\perp , which is the angle between the normal vector of the interface and \mathbf{e}_x -direction; $\theta = \theta_\perp + \pi/2$. The ECS is derived from $\gamma^*(\theta_\perp)$ via Wulff's construction as [1]

$$\Lambda \mathbf{R} = \begin{pmatrix} \cos \theta_\perp & -\sin \theta_\perp \\ \sin \theta_\perp & \cos \theta_\perp \end{pmatrix} \begin{pmatrix} \gamma^*(\theta_\perp) \\ \frac{d}{d\theta_\perp} \gamma^*(\theta_\perp) \end{pmatrix}, \quad (4.2)$$

where $\mathbf{R} = (X, Y)$ is the position vector of a point on the ECS, and Λ a scale factor adjusted to yield the volume (or area) of the crystal. Because ξ calculated in section 3 gives γ^* via the relation (4.1), we can derive the ECS by using (4.2) with suitably chosen Λ . Our result is as follows:

$$\Lambda \mathbf{R} = \begin{pmatrix} -\ln |k \operatorname{sn}(\phi + b \frac{iI'}{4}) \operatorname{sn}(\phi - b \frac{iI'}{4})| \\ -\ln |k \operatorname{sn}(\phi - (2+b) \frac{iI'}{4}) \operatorname{sn}(\phi - (2-b) \frac{iI'}{4})| \end{pmatrix}. \quad (4.3)$$

As ϕ moves from 0 to $2iI'$ on the imaginary axis, \mathbf{R} sweeps out the ECS. One finds that the ECS can be expressed by the algebraic curve of (1.3) with $\alpha = \exp(-\Lambda X)$ and $\beta = \exp(-\Lambda Y)$, where $\bar{A}_2, \bar{A}_3, \bar{A}_4$ are, respectively, given as

$$\bar{A}_2 = \frac{2 \operatorname{cn}(b \frac{iI'}{2}) \operatorname{dn}(b \frac{iI'}{2})}{1 + k \operatorname{sn}(b \frac{iI'}{2})^2}, \quad \bar{A}_3 = 1, \quad \bar{A}_4 = -\frac{(k^{\frac{1}{2}} + k^{-\frac{1}{2}})^2}{1 + k \operatorname{sn}(b \frac{iI'}{2})^2}. \quad (4.4)$$

It follows that the ECS in the Q -state Potts model is the same as those of the Ising model on the Union Jack and 4-8 lattices [23].

Table 2. The elliptic modulus (k) dependence of the interfacial tension (4.1) and the radius of the curvature (4.5) in the facet ($\theta_{\perp} = 0$) and the corner ($\theta_{\perp} = \frac{\pi}{4}$) directions. The parenthesized digits include errors. t^* denotes a reduced temperature related via the duality condition with t .

Q	t	t^*	k	$\gamma^*/k_{\text{B}}T^*$		$\rho/ \mathbf{R} $	
				$\theta_{\perp} = 0$	$\theta_{\perp} = \frac{\pi}{4}$	$\theta_{\perp} = 0$	$\theta_{\perp} = \frac{\pi}{4}$
1	0.50	n/a	0.59350(7)	0.362486	0.363561	1.02403(3)	0.97666(8)
	0.65		0.50773(0)	0.470826	0.473148	1.04036(3)	0.96157(8)
	1.00		0.365456	0.697678	0.705009	1.088221	0.920559
	1.50		0.245846	0.96671(8)	0.985525	1.17049(2)	0.85956(6)
	2.00		0.176466	1.186917	1.220651	1.26045(7)	0.803824
	3.00		0.103562	1.53028(5)	1.59888(8)	1.44810(7)	0.713801
	5.00		0.048141(9)	2.00091(0)	2.14240(7)	1.82311(5)	0.59719(5)
	14.00		0.0081734(7)	3.00755(3)	3.39836(7)	3.3610(2)	0.409052
2	0.24	0.180449	0.59624(2)	0.364650	0.365654	1.022308	0.978298
	0.30	0.212423	0.534544	0.441115	0.442888	1.032748	0.968541
	0.50	0.296641	0.386861	0.665509	0.671532	1.075470	0.931052
	1.00	0.423400	0.207107	1.08788(3)	1.11335(3)	1.20925(6)	0.834354
	2.00	0.542189	0.088825(3)	1.631399	1.711964	1.506487	0.691295
	10.00	0.726099	0.0064337(4)	3.13772(6)	3.56820(1)	3.6663(5)	0.391270
	3	0.15	0.123678	0.5927(1)	0.373112	0.374114	1.02175(2)
0.20		0.155806	0.52116(8)	0.463792	0.465721	1.03390(3)	0.96747(7)
0.30		0.210524	0.41484(1)	0.623150	0.62783(6)	1.06226(7)	0.94224(2)
0.50		0.293001	0.28411(6)	0.88258(8)	0.89586(3)	1.12904(6)	0.88896(2)
1.00		0.416299	0.141663	1.341439	1.386896	1.31958(6)	0.77230(0)
2.00		0.531350	0.057265(5)	1.90363(4)	2.02536(0)	1.71439(4)	0.62527(4)
8.00		0.692933	0.0057675(6)	3.19703(8)	3.64592(6)	3.81500(2)	0.383675
4		0.10	0.087335	0.5983(6)	0.370106	0.371023	1.02004(5)
	0.14	0.116378	0.52232(4)	0.46650(7)	0.46835(9)	1.03233(1)	0.96892(8)
	0.20	0.155063	0.43645(7)	0.59271(5)	0.59654(4)	1.053237	0.950094
	0.30	0.209177	0.33772(6)	0.77034(8)	0.77882(1)	1.092567	0.917077
	0.50	0.290435	0.22315(0)	1.05034(5)	1.07187(5)	1.1806(3)	0.8528(6)
	1.00	0.411331	0.106277	1.52880(7)	1.59378(2)	1.41983(3)	0.72589(3)
	2.00	0.523800	0.0413266	2.10016(8)	2.25771(2)	1.898554	0.580533
	6.00	0.656712	0.0066875(1)	3.11818(1)	3.54183(4)	3.60907(9)	0.394535

We can prove that with the increase of Q but keeping k fixed the interfacial tension (the inverse of correlation length) becomes larger in all directions. In the zero temperature, we expect that the ECS is a square, and exhibits a facet and a corner at $\theta_{\perp} = 0$ and $\pi/4$, respectively. In these directions $\Lambda\mathbf{R} = \gamma^*(\cos\theta_{\perp}, \sin\theta_{\perp})$, so that the radius of curvature ρ is simply given by

$$\frac{\rho}{|\mathbf{R}|} = \left(1 + \frac{1}{\gamma^*} \frac{d^2}{d\theta_{\perp}^2} \gamma^*\right), \quad \theta_{\perp} = 0, \pi/4. \quad (4.5)$$

Though we cannot give such an exact prediction on a Q dependence of the radius of the

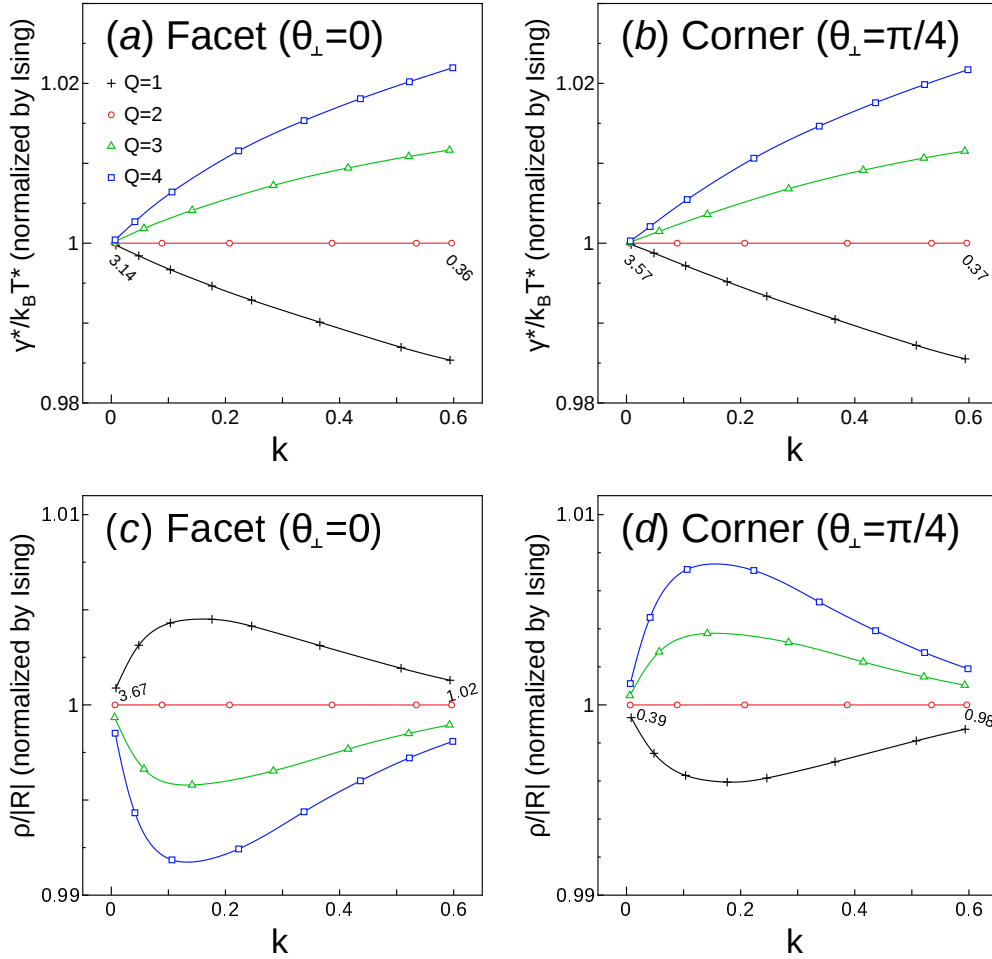


Figure 4. Elliptic modulus (k) dependence of the interfacial tension and the radius of the curvature in the facet ($\theta_{\perp} = 0$) and the corner ($\theta_{\perp} = \frac{\pi}{4}$) directions. The correspondence between marks and Q is provided in the panel (a); the fitting curves are given as a guide for eyes. The figures plot the normalized data by the theoretical Ising values, which are calculated for given k by taking $b = 1$ in (4.1) and (4.5). The bare Ising values are also given by numerals (see table 2).

curvature, we can proffer the numerical data of $\gamma^*/k_{\text{B}}T^*$ and $\rho/|\mathbf{R}|$ at $\theta_{\perp} = 0$ and $\pi/4$, which are then applied to indicate that the ECS is approximated more to a circular shape as Q increases. We summarize our results in table 2. Because their Q dependence is small (up to a few percent), we normalize the bare data using the theoretical Ising values obtained for given k by taking $b = 1$ in (4.1) and (4.5) to make it clearly visible. Figure 4 plots the normalized data. Apparently, from panels (a) and (b), with the increase of Q but keeping k fixed, monotonically the correlation length becomes shorter in both directions, which is in accord with the exact prediction. However, the Q dependence of $\rho/|\mathbf{R}|$ at $\theta_{\perp} = 0$ is opposite to that at $\theta_{\perp} = \pi/4$ [see panels (c) and (d)]: Namely, with the increase of Q the radius of the curvature becomes smaller at $\theta_{\perp} = 0$, but it becomes larger at $\theta_{\perp} = \pi/4$. Intriguingly, this means that the ECS of the Q -state Potts model becomes more rounded in the facet direction, and simultaneously becomes flatter

in the corner direction. Consequently, the ECS is monotonically approximated more to a circular shape with the increase of Q . Moreover, this Q dependence of shape can be extended into the $Q \geq 1$ cases with the ECS replaced by the polar plot of $1/\xi$.

We stress that results uncovered here sharply contrast with those of typical models; namely, when the correlation length of the system becomes larger, the ECS or polar plot of $1/\xi$ usually becomes more circular. One should note that the unusual situation also occurs in the Ising model on the Union Jack and 4-8 lattices [18].

The structure of the elliptic curves in the result (II) also appears in the asymptotic correlation function of the eight-vertex (8V) model [22]. Continuously variable exponents in the 8V model can be explained by the weak universality concept [54], where the inverse correlation length $1/\xi$ is regarded as a variable measuring departure from criticality. Our observation implies that the elliptic modulus k describing the ACL is more essential than $1/\xi$ to parameterize the deviation from T_C . That is, even if they have different values of $1/\xi$ (or γ^*), the models sharing the same value of k are the same in the amount of the deviation from T_C .

We point out that the algebraic geometry can provide a framework to denote this kind of equivalence among models. The algebraic curve (1.3) is a singular curve possessing two nodes at infinity, and the algebraic geometry offers a standard procedure to treat such curves. One possible scenario in this direction is that the weak universality concept in physics can be connected with the bi-rational equivalence of algebraic geometry [40]. We expect that this viewpoint will break new ground in the study of statistical models.

In this paper, we have restricted ourselves to the models defined on the square lattice. However, it is natural to expect that the same situation occurs for other lattices, e.g., a triangular, a honeycomb, and so on. Thus, an extension of our form for other point groups, e.g., C_{6v} is important [23, 24, 25, 26, 27, 28]. Furthermore, all the treated models possess discrete degrees of freedom on lattice points. Thus, it is desired to investigate asymptotic correlation functions of continuous spin models, e.g., the classical XY model by employing the same approach. We will report our studies on these topics to clarify the degree of universality of our form in future.

Acknowledgments

We would like to thank Professors Macoto Kikuchi and Yutaka Okabe for stimulating discussions. We would especially like to dedicate this paper to the 60-th birthday of MK. The main computations were performed using the facilities in Tohoku University and Tokyo Metropolitan University. This research was supported by a grant-in-aid from KAKENHI No. 26400399.

Appendix A.

In this appendix, using (2.10)-(2.16) we determine the form of $L(u)$ defined by (2.24). When N becomes large and $-I'/2 < \Re(u) < I'/2$, the first term is dominant on the rhs of (2.12). We keep only the dominant term there. Divide both sides of (2.12) by $\kappa(u)^N \kappa(u+I')^N$, use (2.14), (2.15), and (2.24), and combine the result from the second equation of (2.10), then we obtain

$$L(u)L(u+I') = 1, \quad L(u-2iI) = rL(u) \quad \text{for } T > T_C. \quad (\text{A.1})$$

Similarly, from (2.13) and the second equation of (2.11), we obtain

$$L(u)L(u+I') = 1, \quad L(u-2iI) = L(u) \quad \text{for } T < T_C. \quad (\text{A.2})$$

Because the zeros of $\Lambda_0(u)$ are located on the line $\Re(u) = -I'/2$ in a periodic rectangle, the first equation of (A.1) or (A.2) shows that the limiting function is written as

$$L(u) = F(u) \prod_{l=1}^{\nu} \frac{a - xa_l}{a - x^3 a_l}, \quad -\frac{I'}{2} < \Re(u) \leq \frac{3I'}{2} \quad (\text{A.3})$$

with $a = \exp(-\pi u/I)$, $a_l = \exp(i\pi\phi_l/I)$, and $x = \exp(-\pi I'/2I)$. A function $F(u)$ is analytic and non-zero for $-I'/2 < \Re(u) \leq 3I'/2$. Thus, the limiting functions are labeled by an integer ν and real numbers $\phi_1, \phi_2, \dots, \phi_\nu$ instead of p . Substitute (A.3) into the first equation of (A.1) or (A.2), take the logarithms of both sides, and then expand them in the annulus $-I'/2 < \Re(u) < I'/2$ using the form

$$\ln F(u) = c_0 + \alpha \ln a + \sum_{\mu=1}^{\infty} (c_\mu a^\mu + c_{-\mu} a^{-\mu}), \quad -\frac{I'}{2} < \Re(u) \leq \frac{3I'}{2}. \quad (\text{A.4})$$

Equating coefficients gives

$$\begin{aligned} \alpha &= \frac{1}{2}\nu, \quad c_0 = -\frac{1}{2} \sum_{l=1}^{\nu} \ln(-a_l), \quad c_\mu = \frac{x^\mu}{1+x^{2\mu}} \frac{1}{\mu} \sum_{l=1}^{\nu} a_l^{-\mu}, \\ c_{-\mu} &= -\frac{x^{3\mu}}{1+x^{-2\mu}} \frac{1}{\mu} \sum_{l=1}^{\nu} a_l^\mu, \quad \mu = 1, 2, \dots \end{aligned} \quad (\text{A.5})$$

Then, we find that

$$L(u) = \pm \prod_{l=1}^{\nu} k^{\frac{1}{2}} \text{sn}(iu - \phi_l - \frac{iI'}{2}), \quad -\frac{I'}{2} < \Re(u) \leq \frac{3I'}{2}. \quad (\text{A.6})$$

For $T > T_C$, from the second equation of (A.1), ν is an odd (even) integer if $r = -1$ ($r = +1$). The next-largest eigenvalues correspond to the case with $\nu = 1$ and $r = -1$.

For $T < T_C$, the two largest eigenvalues $\Lambda_0(u)^2$ and $\Lambda_1(u)^2$ are asymptotically degenerate when N becomes large. Note that $r = +1$ for $\Lambda_0(u)^2$ and $r = -1$ for $\Lambda_1(u)^2$ (see section 7.10 of [11]). The second equation of (A.2) shows that ν is an even number. We thus find that the next-largest eigenvalues correspond to the cases with $\nu = 2$ and $r = \pm 1$.

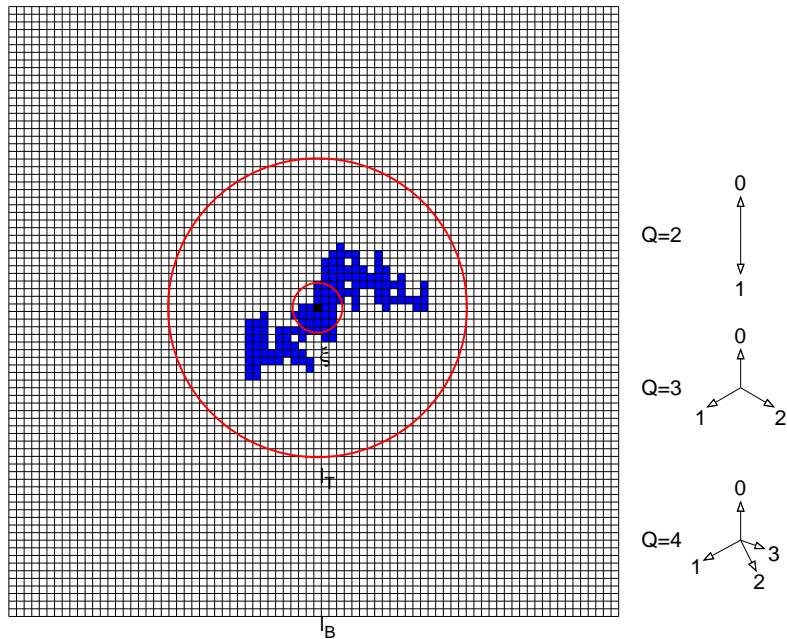


Figure B1. (Left part) Schematic representation of MC simulations. The black cell (the seed site) and blue cells exhibit the FK cluster C_i . The length scales of the bounding box l_B and the equilibrated circular domain l_T as well as the correlation length ξ are depicted. (Right part) We give the magnetic operators by Q unit vectors in $Q - 1$ dimensions, where the corresponding value of $q_{\mathbf{r}}$ is denoted ($Q > 1$). The arrows in the $Q = 3$ ($Q = 4$) case point the corners of the regular triangle (tetrahedron).

Appendix B.

We perform large-scale MC simulation calculations to investigate the correlation functions. In this appendix, we shall detail our methodology. The Hamiltonian of the square-lattice Q -state Potts model is given by (1.1). We treat its isotropic coupling case, i.e., $J_{\mathbf{r},\mathbf{r}'} = 2J$. According to Fortuin and Kasteleyn (FK) [29], the random-cluster representation of the partition function is given as

$$Z(Q) = \text{Tr} e^{-E(Q)/k_B T} = \sum_{\{n\}} p^{\sum_{\mathbf{r}^*} n_{\mathbf{r}^*}} (1-p)^{\sum_{\mathbf{r}^*} (1-n_{\mathbf{r}^*})} Q^{N_c}, \quad (\text{B.1})$$

where $p = 1 - e^{-2K}$ is the bond percolation probability. $n_{\mathbf{r}^*} = 0, 1$ is the bond occupation defined on $\mathbf{r}^* \in \Lambda_{\text{sq}}^*$, and Λ_{sq}^* is the medial-lattice of Λ_{sq} . We denoted the number of FK clusters as N_c . While there are some variations in implementations of cluster MC simulations [55, 56, 57, 46], we employ the so-called infinite-system method proposed by Evertz and von del Linden [46]. It is based on Wolff's single-cluster algorithm [57], and enables us to directly simulate infinite off-critical systems, which thus means that an extrapolation of data to the thermodynamic limit is not necessary. As we explained in section 3.1, this advantage is crucial for our purpose.

To make the explanation concrete, let us consider Λ_{sq} in a temperature dependent bounding box of $l_B \times l_B$ (see figure B1). As an initial condition, we take random spin

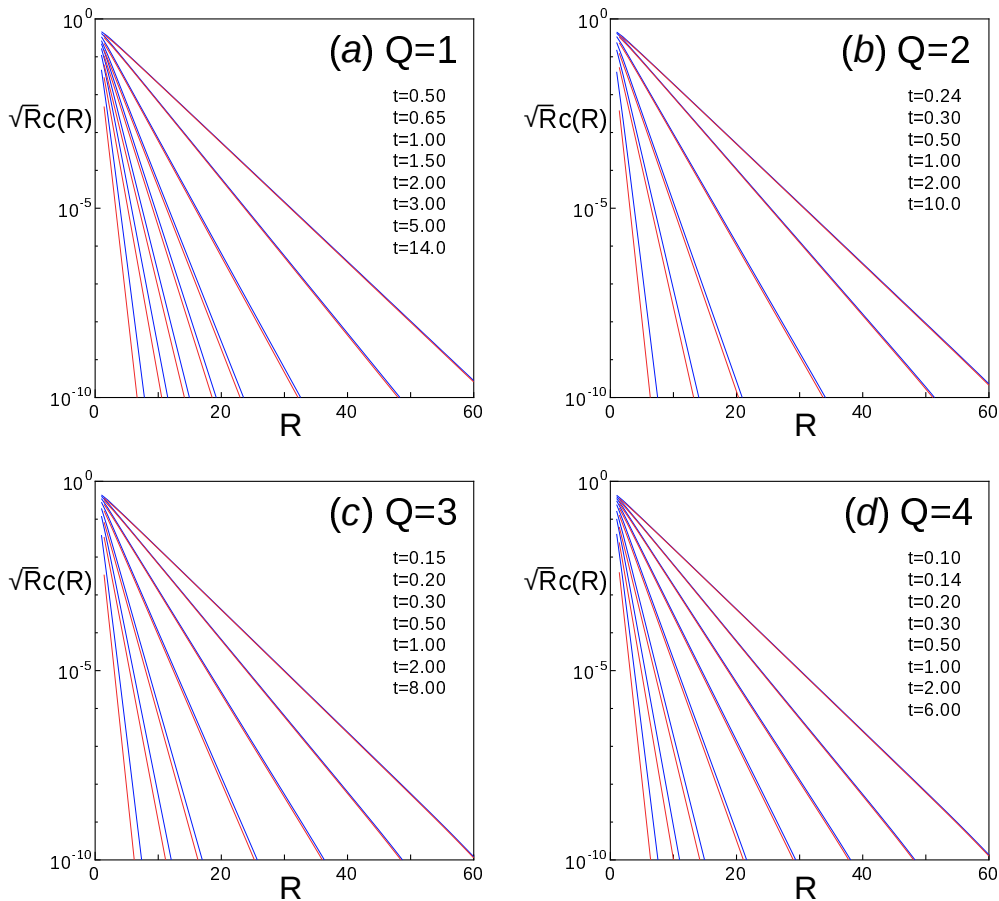


Figure B2. The correlation functions $c(\mathbf{r})$ of the Q -state Potts model in two directions ($Q = 1$ means the bond percolation). For clarity, we draw the lines for MC data points, where the blue (red) ones show $\sqrt{R}c(R)$ in the row-to-row (diagonal) direction: $\mathbf{r} = R\mathbf{e}_x$ [$\mathbf{r} = R(\mathbf{e}_x + \mathbf{e}_y)/\sqrt{2}$]. With the increase of the temperature t , the slopes of lines become steeper, and the deviations between blue and red lines become larger.

configurations instead of “staggered spin configuration” [46] because they are neutral and unbiased for all spin states, and also prevent a deep penetration of clusters toward the boundary (see below). We fix the seed of the cluster to the origin (the black cell), and perform single cluster updates in order to equilibrate a circular domain. Suppose that l_T is its linear dimension. Then, the required number of updates for its equilibration increases exponentially with l_T because the off-critical system possesses finite correlation length ξ . Roughly speaking, we performed equilibration steps to typically realize $l_T \simeq 20 \times \xi$, and also use the bounding box with $l_B > 4 \times l_T$, where the probability that a cluster touches the bounding box is negligible. Consequently, we can perform measurements of the physical quantity, i.e., correlation functions within the circular domain of l_T without finite-size effects [46].

With respect to the measurement of correlation functions, we can benefit from the so-called improved estimators. In the present case, the correlation function of the Potts model $c(\mathbf{r} - \mathbf{r}') := \langle \sigma_{\mathbf{r}} \sigma_{\mathbf{r}'} \rangle$ can be calculated as an average over the FK clusters generated

by MC, i.e., $c(\mathbf{r} - \mathbf{r}') = \langle (\sigma_{\mathbf{r}} \sigma_{\mathbf{r}'})_{\text{impr}} \rangle_{\text{MC}}$, where

$$(\sigma_{\mathbf{r}} \sigma_{\mathbf{r}'})_{\text{impr}} := \frac{1}{|C_i|} \delta(\mathbf{r}, \mathbf{r}' | C_i). \quad (\text{B.2})$$

The set of sites (the number of sites) in a i -th cluster were denoted as C_i ($|C_i|$), and then $\delta(\mathbf{r}, \mathbf{r}' | C_i) = 1$ for $\mathbf{r}, \mathbf{r}' \in C_i$, otherwise zero.

The correspondence between $q_{\mathbf{r}}$ and the magnetic operators is depicted in the right part of figure B1. These magnetic operators can be characterized by the scaling dimensions $x(Q)$, i.e., $x(2) = \frac{1}{8}$, $x(3) = \frac{2}{15}$, $x(4) = \frac{1}{8}$, and also $x(1) = \frac{5}{48}$, which determine the power-law behavior of $c(R)$ at $T_C(Q)$ [49, 58]. The fact that (B.2) is positive definite is crucial for calculations of vanishing correlations for large $R/\xi \gg 1$.

For $T > T_C(Q)$, we shall provide the raw MC data of short-ranged correlation functions in two directions. In figure B2, we exhibit the semi-log plots of correlation functions at various temperatures $t = [T - T_C(Q)]/T_C(Q)$. The pairs of blue and red lines give $\sqrt{R}c(R)$ in the row-to-row ($\mathbf{r} = R\mathbf{e}_x$) and the diagonal [$\mathbf{r} = R(\mathbf{e}_x + \mathbf{e}_y)/\sqrt{2}$] directions. Then, one finds that their slopes become steeper, and the discrepancy of the pair of lines becomes larger with the increase of the reduced temperature t . For exactly solved cases, it was revealed that the correlation length is isotropic near critical point, but becomes anisotropic with distance from it due to the lattice effects. With this in mind, if we suppose the simple form of the correlation function as $c(R) \propto e^{-R/\xi}/\sqrt{R}$, our MC data indicate that ξ in the row-to-row direction is longer than that in the diagonal direction in qualitative agreement with them [8]. Simultaneously, one may notice that the directional dependence of ξ is quite weak, so the extremely accurate data are required for the numerical investigation of the ACLs.

Appendix C.

In this appendix, we detail a fitting procedure of our form (3.2) to the correlation function data provided by the MC simulation calculations. As explained in Appendix B, the infinite-system MC method and the improved estimator for the correlation functions has been employed. In typical cases, we performed 1,000 independent runs of MC simulations, and generated the 10^{11} Fortuin-Kasteleyn clusters at each run. Then, for square-lattice sites $i\mathbf{e}_x + j\mathbf{e}_y \in \Lambda_{\text{sq}}$ within the equilibrated circular domain $R < l_T$ the correlation function data $\{c(i, j)\}$ were obtained, and their statistical errors $\{d(i, j)\}$ were estimated from standard deviations of the averages of the independent runs.

As mentioned in section 3.1, there exist two sources of errors: the systematic errors stemming from higher bands of eigenvalues which are not taken into account in (3.2) and the statistical errors associated with MC samplings. The former (respectively latter) becomes larger inward (respectively outward). We analyze $\{c(i, j)\}$ and $\{d(i, j)\}$ in annular regions $\mathcal{D}(c_{\text{max}}, c_{\text{max}})$ following the procedure explained below.

We shall take the $Q = 3$ and $t = 0.15$ case as an example. In section 3.3, we order-estimated the systematic error as $\Delta(3) \times e^{-2R/\bar{\xi}}$ with $\bar{\xi} \simeq 2.7$ and $\Delta(3) = 1.0 - (A/\pi)(1 - k^2)^{\frac{1}{4}} \times 2I \simeq O(10^{-2})$. Therefore, to calculate the ACL within a five-digit

Table C1. The \mathcal{D}_α -dependence of the estimates of ξ_{diag} and the reduced χ^2 values (see text). Other than the optimized region (\mathcal{D}_0), one inner region (\mathcal{D}_{-1}), and two outer regions (\mathcal{D}_1 and \mathcal{D}_2) are defined by c_{max} and c_{min} at each Q and t . R_α is the mean radius of annular region \mathcal{D}_α .

Q	t	\mathcal{D}_α	c_{max}	c_{min}	$ \mathcal{D}_\alpha $	R_α	ξ_{diag}	$\bar{\chi}_{ \mathcal{D}_\alpha }^2$
1	0.50	\mathcal{D}_{-1}	1×10^{-2}	2×10^{-3}	432	11.9	2.75067(0)	865
		\mathcal{D}_0	1×10^{-4}	3×10^{-5}	436	22.1	2.75056(9)	0.642
		\mathcal{D}_1	1×10^{-5}	4×10^{-6}	392	27.7	2.75056(4)	0.329
		\mathcal{D}_2	5×10^{-8}	3×10^{-8}	336	41.2	2.750(7)	1.231
2	0.24	\mathcal{D}_{-1}	1×10^{-2}	3×10^{-3}	188	10.3	2.73482(4)	0.084
		\mathcal{D}_0	1×10^{-3}	3×10^{-4}	308	16.0	2.73482(3)	0.499
		\mathcal{D}_1	3×10^{-5}	1×10^{-5}	452	24.9	2.7348(4)	0.560
		\mathcal{D}_2	1×10^{-7}	5×10^{-8}	444	39.3	2.734(8)	0.849
3	0.15	\mathcal{D}_{-1}	1×10^{-2}	1×10^{-3}	400	11.5	2.67276(2)	240
		\mathcal{D}_0	1×10^{-4}	3×10^{-5}	400	21.3	2.67297(9)	1.10
		\mathcal{D}_1	2×10^{-6}	1×10^{-6}	368	30.6	2.6729(1)	0.810
		\mathcal{D}_2	1×10^{-7}	5×10^{-8}	436	38.3	2.6728(5)	0.496
4	0.10	\mathcal{D}_{-1}	1×10^{-2}	1×10^{-3}	400	11.5	2.69457(7)	758
		\mathcal{D}_0	3×10^{-5}	1×10^{-5}	428	24.3	2.69525(2)	0.301
		\mathcal{D}_1	2×10^{-6}	1×10^{-6}	348	30.7	2.6952(5)	0.114
		\mathcal{D}_2	1×10^{-7}	5×10^{-8}	452	38.5	2.695(1)	0.223

accuracy, we need to employ an annular region with mean radius $\simeq 20$ or longer. Because the statistical errors are larger in outer regions, we choose $\mathcal{D}_0 = \mathcal{D}(1 \times 10^{-4}, 3 \times 10^{-5})$ with mean radius $R_0 \simeq 21.3$ as an optimized region.

Then, we define χ^2 as a function of A , k , b by

$$\chi^2(A, k, b) = \sum_{(i,j) \in \mathcal{D}_0} \left[\frac{\mathcal{F}_{\text{sq}}(i, j; A, k, b) - c(i, j)}{d(i, j)} \right]^2, \quad (\text{C.1})$$

We extract values \bar{A} , \bar{k} , and \bar{b} of the fitting parameters by minimizing $\chi^2(A, k, b)$. The first line of the third part in table 1 gives their estimates and also the parentheses showing digits including errors, which were put based on differences between two results to two groups of independent runs (e.g., we divided 1,000 independent runs into two groups, and performed fitting calculation for each).

We have expected the extracted values to be obtained under a well-controlled condition of systematic errors by carefully choosing the fitting region. To show concrete evidence to this statement, we perform fittings of data in different annular regions \mathcal{D}_α , and check the \mathcal{D}_α -dependence of an estimate as well as a reduced χ^2 values, i.e.,

$$\bar{\chi}_{|\mathcal{D}_\alpha|}^2 = \frac{\chi^2(\bar{A}, \bar{k}, \bar{b})}{|\mathcal{D}_\alpha|}. \quad (\text{C.2})$$

The third part of table C1 compares the estimates in one inner region (\mathcal{D}_{-1}), the optimized region (\mathcal{D}_0), and two outer regions (\mathcal{D}_1 and \mathcal{D}_2). In general, $\bar{\chi}_{|\mathcal{D}_\alpha|}^2$ measures

the goodness of fit, which in the present case gives an applicability condition of (3.2) to MC data in \mathcal{D}_α . First, one sees that $\bar{\chi}_{|\mathcal{D}_{-1}|}^2$ is much larger than the others, and that ξ_{diag} estimated in \mathcal{D}_{-1} deviates largely from those in other regions. Meanwhile, the error in ξ_{diag} shown by parenthesized digits becomes smaller for \mathcal{D}_{-1} . These show that (3.2) cannot fit the data in \mathcal{D}_{-1} due to the systematic errors. Second, one also finds that $\bar{\chi}_{|\mathcal{D}_1|}^2$ and $\bar{\chi}_{|\mathcal{D}_2|}^2$ are comparable to $\bar{\chi}_{|\mathcal{D}_0|}^2$, and that the estimates of ξ_{diag} are almost independent of the choice of the outer regions. Therefore, we conclude that \mathcal{D}_0 , \mathcal{D}_1 , and \mathcal{D}_2 are in an asymptotic region in which (3.2) can be used for the fitting under the controlled condition of systematic errors, but the statistical errors become larger in outer region.

The first, the second, and the fourth parts of table C1 give the results obtained via the same analysis for the $Q = 1$, $t = 0.50$, the $Q = 2$, $t = 0.24$, and the $Q = 4$, $t = 0.10$ cases, respectively. While overall feature of $Q = 1, 4$ is same as that of $Q = 3$, the fitting condition for $Q = 2$ is clearly different from them, namely, both $\bar{\chi}_{|\mathcal{D}_\alpha|}^2$ and ξ_{diag} are almost independent of \mathcal{D}_α . This difference can be attributed to the presence/absence of the second-band-eigenvalue contributions to the correlation function: As explained in section 2.2, they are absent in the Ising case so that (3.2) can fit the data in inner annular regions like \mathcal{D}_{-1} .

Table 1 exhibits the fitting data in optimized regions \mathcal{D}_0 for which the convergence check of estimates as demonstrated in table C1 had been performed at all temperatures. In principle, we can employ a wider annular region including, e.g., \mathcal{D}_0 , \mathcal{D}_1 , and \mathcal{D}_2 , but, in reality the infinite-system algorithm MC simulations cannot provide reliable averages and meaningful errors for $R \gg \xi_{\text{diag}}$ within a moderate computational effort [46]. Therefore, the optimization of the fitting region is necessary for purpose of the accurate estimations of the ACLs.

References

- [1] G. Wulff. Zur frage der geschwindigkeit des wachstums und der auflösung der krystallflächen. *Z. Krist. Mineral.*, 34:449–530, 1901.
- [2] W. K. Burton, N. Cabrera, and F. C. Frank. The growth of crystals and the equilibrium structure of their surfaces. *Philos. Trans. R. Soc. London, Ser. A*, 243(866):299–358, 1951.
- [3] C. Rottman and M. Wortis. Exact equilibrium crystal shapes at nonzero temperature in two dimensions. *Phys. Rev. B*, 24:6274–6277, Dec 1981.
- [4] J. E. Avron, H. van Beijeren, L. S. Schulman, and R. K. P. Zia. Roughening transition, surface tension and equilibrium droplet shapes in a two-dimensional ising system. *J. Phys. A: Math. Gen.*, 15(2):L81, 1982.
- [5] R. K. P. Zia and J. E. Avron. Total surface energy and equilibrium shapes: Exact results for the $d = 2$ ising crystal. *Phys. Rev. B*, 25:2042–2045, Feb 1982.
- [6] Henk van Beijeren. Exactly solvable model for the roughening transition of a crystal surface. *Phys. Rev. Lett.*, 38:993–996, May 1977.
- [7] C. Jayaprakash, W. F. Saam, and S. Teitel. Roughening and facet formation in crystals. *Phys. Rev. Lett.*, 50:2017–2020, Jun 1983.
- [8] M. Fujimoto. Equilibrium crystal shape of the potts model at the first-order transition point. *J. Phys. A: Math. Gen.*, 30(11):3779, 1997.
- [9] M. Fujimoto. Eight-vertex model: Anisotropic interfacial tension and equilibrium crystal shape. *J. Stat. Phys.*, 67(1):123–154, Apr 1992.
- [10] M. Fujimoto. Equilibrium crystal shape of hard squares with diagonal attractions. *J. Phys. A: Math. Gen.*, 26(10):2285, 1993.
- [11] R. J. Baxter. *Exactly Solved Models in Statistical Mechanics*. Academic Press, London, 1982.
- [12] F. Y. Wu. The potts model. *Rev. Mod. Phys.*, 54:235–268, Jan 1982.
- [13] R. J. Baxter. Potts model at the critical temperature. *J. Phys. C: Solid State Phys.*, 6(23):L445, 1973.
- [14] A. Klümper, A. Schadschneider, and J. Zittartz. Inversion relations, phase transitions and transfer matrix excitations for special spin models in two dimensions. *Z. Phys. B*, 76(2):247–258, Jun 1989.
- [15] E. Buddenoir and S. Wallon. The correlation length of the potts model at the first-order transition point. *Journal of Physics A: Mathematical and General*, 26(13):3045–3062, jul 1993.
- [16] R. K. P. Zia. Duality of interfacial energies and correlation functions. *Physics Letters A*, 64(4):345 – 347, 1978.
- [17] L. Laanait. Discontinuity of surface tensions in the q -state potts model. *Physics Letters A*, 124(9):480 – 484, 1987.
- [18] M. Holzer. Equilibrium crystal shapes and correlation lengths: A general exact result in two dimensions. *Phys. Rev. Lett.*, 64:653–656, Feb 1990.
- [19] Yasuhiro Akutsu and Noriko Akutsu. Interface tension, equilibrium crystal shape, and imaginary zeros of partition function: Planar ising systems. *Phys. Rev. Lett.*, 64:1189–1192, Mar 1990.
- [20] S. B. Rutkevich. Comment on 'equilibrium crystal shape of the potts model at the first-order transition point'. *J. Phys. A: Math. Gen.*, 35(34):7549, 2002.
- [21] M. Fujimoto. Reply to 'comment on "equilibrium crystal shape of the potts model at the first-order transition point"'. *J. Phys. A: Math. Gen.*, 35(34):7553, 2002.
- [22] M. Fujimoto. Anisotropic correlation length in the eight-vertex model. *Physica A*, 233(1):485 – 502, 1996.
- [23] M. Holzer. Exact equilibrium crystal shapes in two dimensions for free-fermion models. *Phys. Rev. B*, 42:10570–10582, Dec 1990.
- [24] H. G. Vaidya. The spin-spin correlation functions and susceptibility amplitudes for the two-dimensional ising model; triangular lattice. *Physics Letters A*, 57(1):1 – 4, 1976.
- [25] R. K. P. Zia. Exact equilibrium shapes of ising crystals on triangular/honeycomb lattices. *J. Stat.*

- Phys.*, 45(5):801–813, Dec 1986.
- [26] M. Fujimoto. Duality relations and equilibrium crystal shapes of potts models on triangular and honeycomb lattices. *Physica A*, 264(1):149 – 170, 1999.
 - [27] M. Fujimoto. Auxiliary vertices method for kagomé-lattice eight-vertex model. *J. Stat. Phys.*, 90(1):363–388, Jan 1998.
 - [28] M. Fujimoto. Anisotropic interfacial tension and the equilibrium crystal shape of kagomé-lattice eight-vertex model. *J. Phys. A: Math. Gen.*, 35(7):1517, 2002.
 - [29] C. M. Fortuin and P. W. Kasteleyn. On the random cluster model. 1. introduction and relation to other models. *Physica*, 57:536–564, 1972.
 - [30] B. M. McCoy and T. T. Wu. *The Two-Dimensional Ising Model*. Harvard University Press, Cambridge, Massachusetts, 1973.
 - [31] H. Cheng and T. T. Wu. Theory of toeplitz determinants and the spin correlations of the two-dimensional ising model. iii. *Phys. Rev.*, 164:719–735, Dec 1967.
 - [32] M. Fujimoto. Hard-hexagon model: Anisotropy of correlation length and interfacial tension. *J. Stat. Phys.*, 59(5):1355–1381, Jun 1990.
 - [33] T. T. Wu, B. M. McCoy, C. A. Tracy, and E. Barouch. Spin-spin correlation functions for the two-dimensional ising model: Exact theory in the scaling region. *Phys. Rev. B*, 13:316–374, Jan 1976.
 - [34] K. Yamada. On the Spin-Spin Correlation Function in the Ising Square Lattice and the Zero Field Susceptibility. *Prog. Theor. Phys.*, 71(6):1416–1418, 06 1984.
 - [35] R. J. Baxter. Solvable eight-vertex model on an arbitrary planar lattice. *Philos. Trans. R. Soc. London, Ser. A*, 289(1359):315–346, 1978.
 - [36] J. D. Johnson, S. Krinsky, and B. M. McCoy. Critical index ν of the vertical-arrow correlation length in the eight-vertex model. *Phys. Rev. Lett.*, 29:492–494, Aug 1972.
 - [37] J. D. Johnson, S. Krinsky, and B. M. McCoy. Vertical-arrow correlation length in the eight-vertex model and the low-lying excitations of the $x - y - z$ hamiltonian. *Phys. Rev. A*, 8:2526–2547, Nov 1973.
 - [38] M. Fujimoto. Spatial anisotropy and rotational invariance of critical hard squares. *J. Phys. A: Math. Gen.*, 27(15):5101, 1994.
 - [39] R. J. Baxter. Free-fermion, checkerboard and z -invariant lattice models in statistical mechanics. *Proceedings of the Royal Society of London A: Mathematical, Physical and Engineering Sciences*, 404(1826):1–33, 1986.
 - [40] M. Namba. *Geometry of projective algebraic curves*. Monographs and textbooks in pure and applied mathematics. M. Dekker, 1984.
 - [41] A. Hintermann, H. Kunz, and F. Y. Wu. Exact results for the potts model in two dimensions. *Journal of Statistical Physics*, 19(6):623–632, Dec 1978.
 - [42] W. Janke and S. Kappler. Correlation length of 2d potts models: numerical vs exact results. *Nuclear Physics B - Proceedings Supplements*, 34:674 – 676, 1994. Proceedings of the International Symposium on Lattice Field Theory.
 - [43] W. Janke and S. Kappler. Monte carlo study of cluster-diameter distribution: An observable to estimate correlation lengths. *Phys. Rev. E*, 56:1414–1420, Aug 1997.
 - [44] Yasuhiro Akutsu and Noriko Akutsu. Novel numerical method for studying the equilibrium crystal shape. *J. Phys. Soc. Jpn.*, 56(1):9–12, 1987.
 - [45] Noriko Akutsu and Yasuhiro Akutsu. Equilibrium crystal shape:two dimensions and three dimensions. *J. Phys. Soc. Jpn.*, 56(7):2248–2251, 1987.
 - [46] H. G. Evertz and W. von der Linden. Simulations on infinite-size lattices. *Phys. Rev. Lett.*, 86:5164–5167, May 2001.
 - [47] M. P. M. den Nijs. A relation between the temperature exponents of the eight-vertex and q -state potts model. *Journal of Physics A: Mathematical and General*, 12(10):1857–1868, oct 1979.
 - [48] M. P. Nightingale and H. W. J. Blöte. Finite size scaling and critical point exponents of the potts model. *Physica A: Statistical Mechanics and its Applications*, 104(1):352 – 357, 1980.

- [49] H. W. J. Blöte and M. P. Nightingale. Critical behaviour of the two-dimensional potts model with a continuous number of states; a finite size scaling analysis. *Physica A: Statistical Mechanics and its Applications*, 112(3):405 – 465, 1982.
- [50] A. Aharony and D. Stauffer. *Introduction to percolation theory*. Taylor & Francis, 2003.
- [51] Y. Higuchi. *SUGAKU* (in Japanese), 40(3):247–254, 1988.
- [52] M. Aizenman and D. J. Barsky. Sharpness of the phase transition in percolation models. *Communications in Mathematical Physics*, 108(3):489–526, Sep 1987.
- [53] M. V. Menshikov. Coincidence of critical points in percolation problems. In *Soviet Mathematics Doklady*, volume 33, pages 856–859, 1986.
- [54] M. Suzuki. New universality of critical exponents. *Prog. Theor. Phys.*, 51(6):1992–1993, 1974.
- [55] R. Swendsen and Jian-Sheng Wang. Nonuniversal critical dynamics in monte carlo simulations. *Phys. Rev. Lett.*, 58:86–88, Jan 1987.
- [56] U. Wolff. Lattice field theory as a percolation process. *Phys. Rev. Lett.*, 60:1461–1463, Apr 1988.
- [57] U. Wolff. Collective monte carlo updating for spin systems. *Phys. Rev. Lett.*, 62:361–364, Jan 1989.
- [58] Y. Deng, H. W. J. Blöte, and B. Nienhuis. Backbone exponents of the two-dimensional q -state potts model: A monte carlo investigation. *Phys. Rev. E*, 69:026114, Feb 2004.